8-2023

The Application of Model Predictive Control on Paralleled Converters for Zero Sequence Current Suppression and Active Thermal Management

Justin Dobey
jdobey@g.clemson.edu

The Application of Model Predictive Control on Paralleled Converters for Zero Sequence Current Suppression and Active Thermal Management

---

A Thesis
Presented to
the Graduate School of
Clemson University

In Partial Fulfillment
of the Requirements for the Degree
Master of Science in
Electrical Engineering

---

by
Justin Keyshawn Dobey
August 2023

Accepted by:
Dr. Christopher Edrington, Committee Chair
Dr. Gokhan Ozkan
Dr. Zheyu Zhang

Abstract

In the field of power electronics, the control of rectifiers is a crucial area of study. Rectifiers are used to convert AC power into DC power, and are commonly used in a wide range of applications, including renewable energy systems, industrial automation, and consumer electronics. However, in medium and high-power systems when multiple rectifiers are connected in parallel to a DC bus, stability issues can arise, including voltage fluctuations, zero sequence circulating current, and thermal imbalance.

Achieving stable DC bus voltage is essential for maintaining the proper functioning of electronic devices, while suppressing zero sequence current is necessary for protecting the power electronics equipment from damage and ensuring that a power system's performance is not degraded. Active thermal management is important for ensuring the longevity and reliability of the power electronics equipment.

To achieve these objectives, advanced control techniques must be developed and implemented. This research investigates the use model predictive control to achieve three objectives in two paralleled rectifier each control cycle: DC voltage stability, zero sequence suppression, and thermal balance. These objectives are critical for ensuring the reliable and efficient operation of power electronics systems.

The findings of this research will contribute to the development of more reliable and efficient power electronics systems, with the Navy's (power electronic building block) PEBB systems particularly in mind. However, this research can be extended to other medium and high-powered applications in modern technology too such as missile defense systems, data centers, and uninterruptible power supplies.

Acknowledgments

I would like to express my deepest gratitude to my family, especially my mom Leslie, my dad Johnny, and my brother Jairus, for their support throughout my thesis journey. Their belief in me and constant encouragement kept me motivated and focused.

My heartfelt appreciation goes to my advisors, Dr. Chris Edrington, Dr. Gohkan Ozkan, and Dr. Zheyu Zhang. Dr. Edrington, as my initial point of contact in the Real Time Control and Optimization Laboratory (RT-COOL), played a pivotal role in shaping the direction of my thesis and providing the necessary resources for my academic pursuit. I am truly grateful for his support and mentorship.

Dr. Ozkan's expertise and willingness to assist were crucial in overcoming the challenges I faced during simulations. His patient guidance and insightful suggestions significantly improved the quality of my work, and I am deeply thankful for his ongoing support.

I owe a debt of gratitude to Dr. Zhang, whose passion for teaching power electronics inspired my interest in the subject. Through his captivating lectures, I found the inspiration to join the research group and explore this fascinating field. His teaching has profoundly impacted my academic and research pursuits, and for that, I am truly grateful.

I would also like to thank my high school physics teacher, Mrs. Kathy Gambill, whose engaging and hands-on projects sparked my fascination with engineering. Her dedication to teaching and commitment to nurturing young minds set me on the path towards my passion for engineering, which continues to drive me today.

I am also grateful to my classmates, friends, and previous professors for their support and collaboration. Our insightful discussions enriched my understanding of the subject matter, making the journey more enjoyable.

To all those who have offered words of encouragement or extended a helping hand, your

support has been much appreciated. Your belief in my capabilities and encouragement have been invaluable throughout this academic pursuit.

And to everyone who has been a part of my life, whether mentioned or unmentioned, your impact has been significant. I deeply appreciate your presence, guidance, and the belief you have shown in my abilities. Thank you for contributing to my academic and personal growth and for shaping the person I am today.

Table of Contents

List of Figures

Chapter 1

Introduction

Electronic equipment and devices have become an integral part of modern society. From smartphones and laptops to electric vehicles and renewable energy systems, these devices rely on electric power to function. However, the power supplied by the electrical grid is not always in the required form for these devices, necessitating the use of power electronics. Power electronics is a field of study that deals with the conversion and control of electrical power.

Power electronics technology has been developed to address the challenges of delivering reliable and efficient power to the increasing number of electronic devices in use today. Power electronics converters are utilized to transform electrical power from the grid into a form suitable for electronic devices, such as DC voltage. These converters also enable the control of power flow to meet the demands of devices and equipment.

In the realm of electric power converters, numerous types exist. However, the simultaneous achievement of efficiency, miniaturization, and cost reduction in power converters has been made possible by the invention and rapid development of solid-state devices. Solid-state devices utilize semiconductor materials to control the flow of electric current, enabling them to act as switches. Power converters that utilize solid-state technology for controlling and converting electric power are commonly referred to as switching converters. Figure 1.1 illustrates the basic elements of any switching converter.

Significant advancements in solid-state technology have fueled a growing trend towards increasing power density in power converters. This trend arises from the increasing demand to reduce energy consumption, minimize the size and weight of electronic devices, and enhance their overall

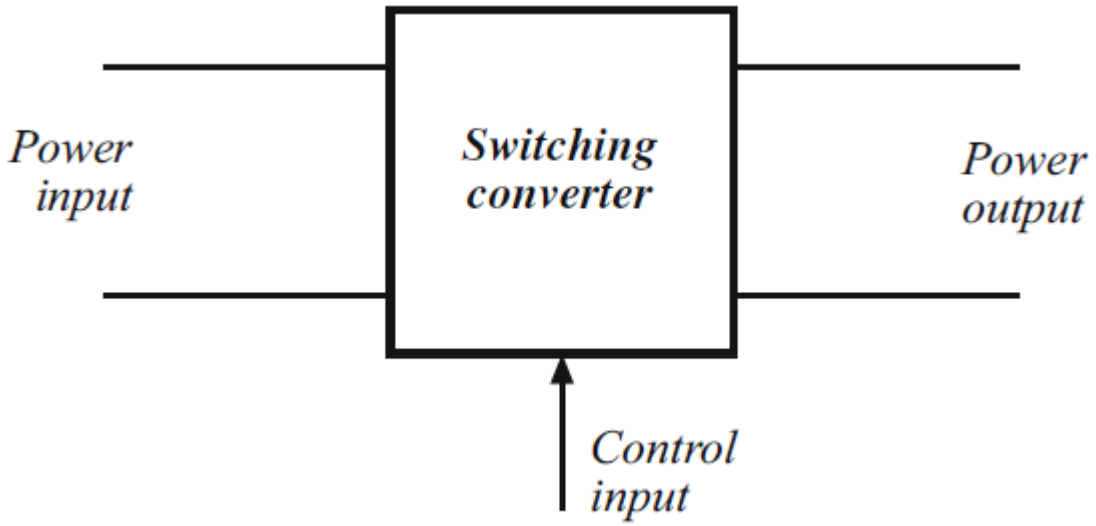

Figure 1.1: The basic elements of any switching converter [12]

reliability. By pushing the boundaries of power density, modern power converters can deliver higher power outputs while occupying minimal physical space. This trend has profound implications for various industries, including the residential, industrial, commercial, medical, communications, transportation, aerospace, and military sectors, where efficient power conversion with reduced footprint and weight is critical for optimal performance.

1.1 Motivation

The motivation behind achieving higher efficiency in power converters lies in the reduction of wasted power, translating to cost and resource savings. One sector that could tremendously benefit from even slightly more efficient power converters is the military, particularly the United States Department of Defense (DOD). As the world's largest institutional user of petroleum, the DOD is also the single largest institutional producer of greenhouse gases [7]. Given the multitude of weapons, buildings, ships, aircraft, and combat vehicles that the DOD must keep operational, both domestically and overseas, achieving energy efficiency is crucial to fulfill its mission of deterring war and ensuring national security.

Recognizing the significant energy consumption and spending, the US Navy has been funding research on power electronics building blocks (PEBBs) at multiple universities and manufac-

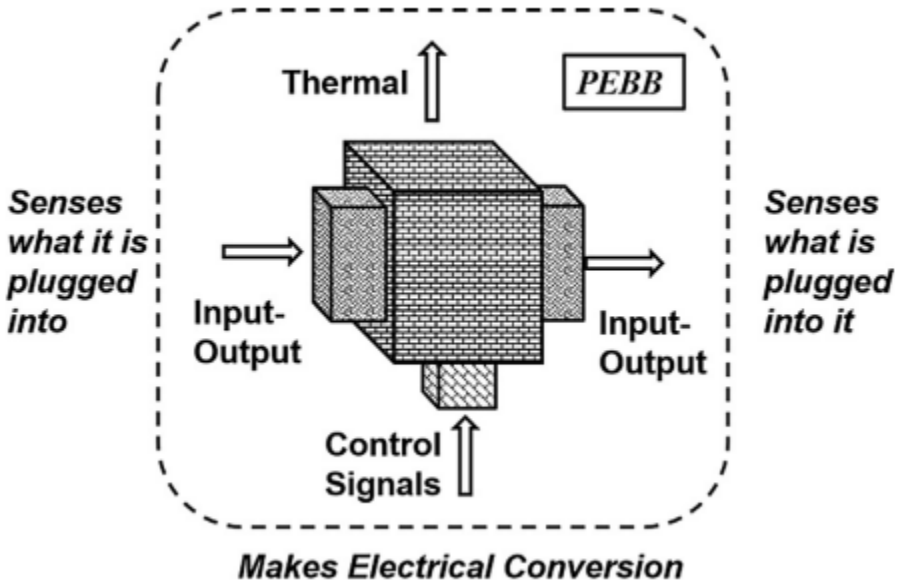

Figure 1.2: Power Electronic Building Block (PEBB) concept [4]

turers [14]. PEBBs are modular power processors capable of converting any input electrical power into a desired voltage, current, and frequency output [13]. The Navy intends to integrate PEBB-based systems into future ships and aircraft as part of their electrification efforts. PEBBs not only enhance system energy efficiency but also reduce engineering effort, design testing, onsite installation, and maintenance for specific applications, thanks to their plug-and-play architecture. Once a PEBB is inserted into a system, its settings are automatically configured, enabling full operational capabilities.

Figure 1.2 presents the basic concept of a power electronic building block (PEBB). The power processing unit occupies the center of the PEBB and can identify the connected input/output terminals, such as a generator, battery, motor, or another PEBB. Additionally, the PEBB incorporates an input control signal and provides a thermal status output signal, which, in conjunction with intelligent control, helps prevent overheating.

While the Navy's focus on PEBBs is primarily for defense purposes, it is worth noting that further research and integration of PEBB-based systems can have a significant impact on the commercial sector as well. In traditional power electronics, each system is designed based on

its specific application, often requiring extensive redesign when upgrading a single component due to potential changes in system power dynamics. However, PEBB-based systems offer modularity, reducing design efforts and component implementation, resulting in faster product release and lower design costs.

PEBB devices can address core cost issues associated with both mature and emerging power technologies. For mature technologies, there is an ongoing demand for cost reduction, which can be achieved through PEBB device standardization. This standardization drives down costs by providing a common product framework. Regarding emerging technologies, reducing research and development costs is essential for companies to generate larger profits. PEBB device standardization allows for the development of building blocks in the power electronics field, rather than starting from scratch for each new application [52].

While PEBB technology holds immense promise, it also presents various challenges. Although this paper does not focus specifically on PEBB technology itself, it addresses problems that can be extended and applied to PEBB technology. Specifically, this paper examines the obstacles that arise when connecting switching converters in parallel, including power imbalance, zero-sequence current, and thermal imbalance. Throughout this thesis, these challenges are thoroughly investigated, and potential solutions for each are explored. By delving into the intricacies of power electronics, the potential for more efficient, reliable, and advanced electronic devices and systems can be unlocked. This thesis aims to contribute to the knowledge and development of power electronics, paving the way for future innovations in this rapidly evolving field.

Chapter 2

Power Electronic Devices

Before delving into the control techniques for addressing power converter issues, it is essential to understand components at the heart of switching converters— semiconductor devices. These devices function as switches, operating in either an ON or OFF state. In the ideal ON state, current flows through the device without any voltage drop, while in the ideal OFF state, no current passes through, but a blocking voltage is present across the device. Under these ideal scenarios, power converter efficiency would approach 100%. Although achieving perfect efficiency is impractical, it is not uncommon for converter efficiencies of 95% or even higher to be achieved under optimum conditions [34]. Converter losses are discussed in more detail later in this chapter.

There are a multitude of power converter circuit topologies that do not require semiconductor devices to function as switches that are either fully turned ON or fully turned OFF, such as linear voltage regulators. These types of converters have switches that operate in their linear region. This means that both current and voltage are present across the device, resulting in significantly higher power losses before the input power is transformed. And because no switching action is involved, larger circuit filters are necessary, further increasing the size and cost of the overall circuit. This topic is further discussed in the following paragraph.

The advantage of using semiconductors as switches lies in their ability to transition between states without the need for mechanical parts. Semiconductor switches can easily turn ON and OFF at frequencies reaching hundreds of thousands of hertz, far surpassing the capabilities of mechanically moving switches. Other notable advantages of semiconductor switches over mechanical switches include power handling capability and reliability. However, system designers often aim for higher

switching frequencies due to their impact on filter components. Filters are a necessity for a power system and are employed in various configurations for different purposes. One crucial reason for their implementation is to suppress voltage and current harmonics associated with switching. If these harmonics are not suppressed and allowed to flow freely into either the input or output of the converter, serious issues may arise. These issues include but are not limited to: degradation of output power quality, reduced power factor, power source instability, increased copper losses in electrical machinery, amplified torque ripple in induction motors, heightened electromagnetic interference, and numerous other potential problems [57]. Designers allow a certain level of voltage and current ripple for the filter capacitors and inductors, respectively. Switching frequency and filter size are inversely related. This means that higher switching frequencies enable the reduction of filter component size while still maintaining the acceptable level of voltage and current ripple [12]. Consequently, smaller filter components contribute to lower weight and cost of the power converter.

2.1 Switching Implementation

To control a switching converter effectively, it is important for the designer to select and understand the most suitable semiconductor switching device. There are numerous options available and there is no single device that serves as the perfect choice for all situations. Different switching devices are commonly employed in modern converters and each has its own trade-offs. For instance, while certain devices offer higher power handling capabilities, there may be compromises in terms of cost and switching speed. Designers must always consider these trade-offs to choose the optimal switching device for their specific application. This section addresses the capabilities and ideal current-voltage (IV) characteristics of some commonly used switching devices. The detailed physics behind the operation of these devices will not be covered extensively.

2.1.1 The Diode

The diode is one of the simplest types of semiconductor switches. Figure 2.1 illustrates its symbol and characteristics. There are various types of diodes, a few of which include light-emitting diodes (LEDs), Schottky diodes, and Zener diodes. However, high-power converters primarily utilize power diodes, which are formed by joining p-type and n-type semiconductor materials. Power diodes can be found in a very wide range of applications with a very wide scale of power ratings. They

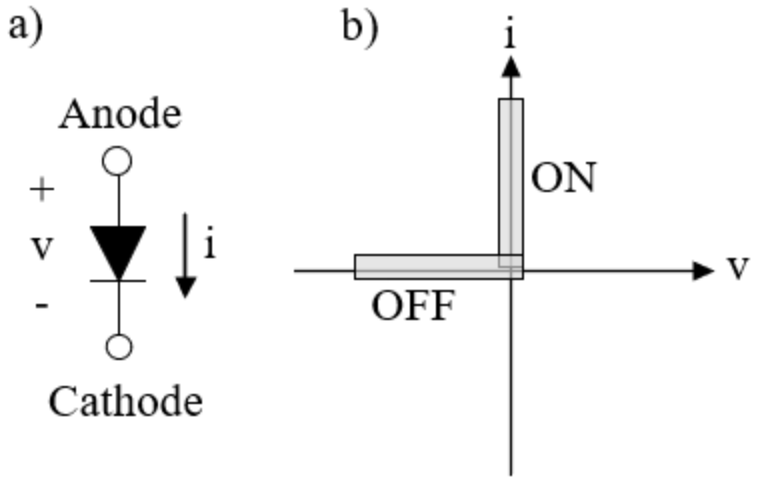

Figure 2.1: The diode symbol (a) and its characteristics (b) [12]

are commonly utilized as uncontrolled switches in AC-to-DC power converters and as freewheeling diodes that protect circuits from voltage spikes caused by inductive loads. The switching capabilities of power diodes range from one millisecond in megawatt applications to hundreds of nanoseconds in milliwatt applications [31]. Higher rated power diodes require longer switching times due to the higher charge density that needs to be displaced at the p-n junction.

Power diodes are considered passive switches because they operate based on the polarity of the voltage and current within a circuit, requiring no control signal to function. They operate in two different modes: forward biased (ON state) and reverse biased (OFF state). In the forward biased mode, the diode acts as a short circuit, allowing current to flow in only one direction— from the anode to the cathode. In the reverse biased mode, the diode acts as an open circuit, preventing any flow of current and blocking any negative voltage.

2.1.2 The BJT

The bipolar junction transistor (BJT) is a fully controlled three-terminal switching device. Its symbol and characteristics are shown in figure 2.2. Like the diode, there are multiple variations of the BJT, but the power BJT is commonly used in higher power electronic applications. When a BJT is connected to a closed circuit, current enters its collector terminal. If a strong enough current signal is present on the base terminal, current will flow out of the device from the emitter terminal. This means that the signal passed to the base terminal acts as a control for the device.

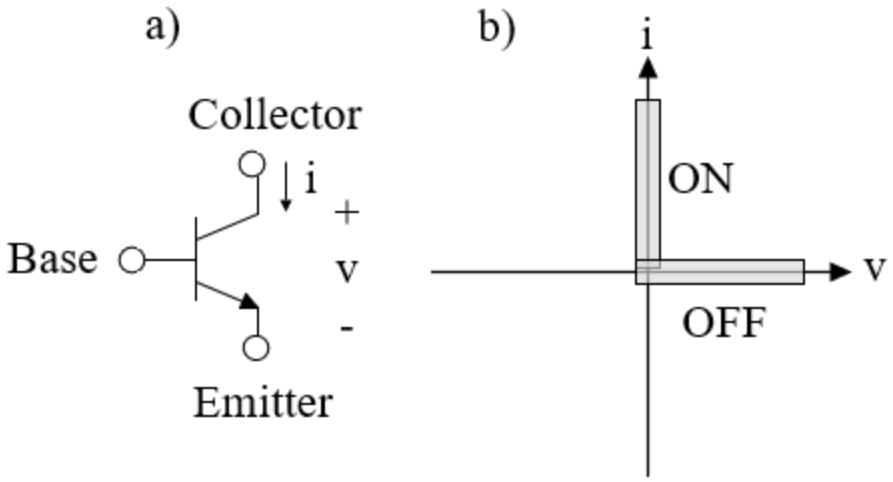

Figure 2.2: The BJT symbol (a) and its characteristics (b) [12]

Also like the diode, the BJT is created through the use of p-n junctions. An NPN-transistor is formed when a thin p-type semiconductor material is sandwiched between two n-type semiconductor materials. A PNP-transistor is formed when a thin n-type semiconductor material is sandwiched between two p-type semiconductor materials. The semiconductor layers of both types of transistors are shown in figure 2.3. Although both types of transistors work in a similar capacity, the NPN-transistor has higher voltage and current ratings, making it better suited for power electronic applications [41].

The BJT is widely used in electronic applications as an amplifier rather than a switch, primarily because of its ability to amplify a small base current to produce a larger collector current [41]. However, the BJT has been largely replaced by the metal oxide semiconductor field-effect transistor (MOSFET) in low-voltage applications and by the insulated-gate bipolar transistor (IGBT) in high-voltage applications due to some of the BJT's inferior device characteristics, such as lower switching speeds. Nevertheless, the BJT will likely never phase out from the power electronics world due is its low cost and decades-long implementation in power electronic systems.

2.1.3 The MOSFET

The MOSFET is another fully controlled semiconductor device. It is by far the most commonly produced type of semiconductor device in today's world. Its symbol and characteristics are

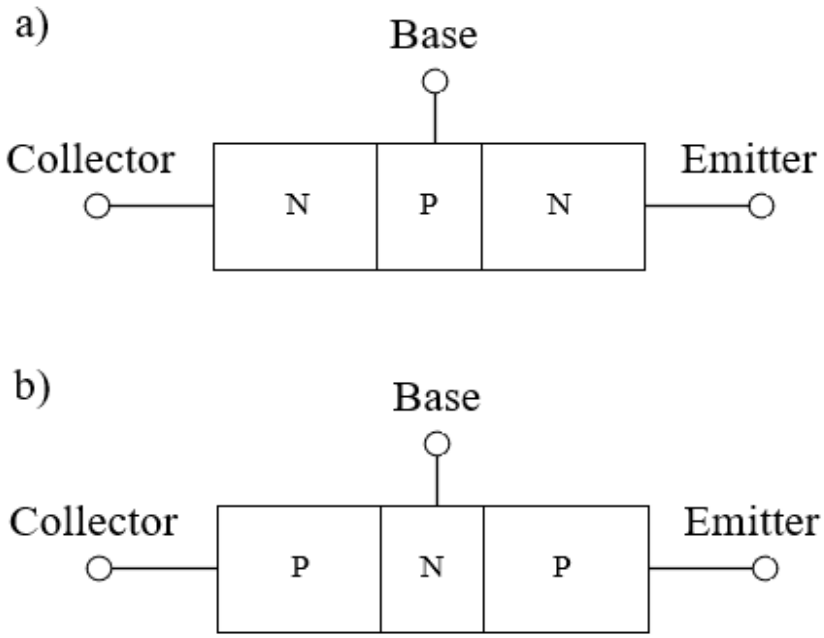

Figure 2.3: The cross-sectional diagrams of the NPN (a) and PNP (b) variations of the BJT

shown in figure 2.4, and its cross-sectional diagram is shown in figure 2.5. Unlike the previously mentioned switches, the MOSFET is a bidirectional switch, allowing current to flow in both directions. This feature is essential for AC power applications where currents of both polarities must flow through the converter, while only one voltage polarity needs to be blocked. However, there are other switches that can fulfill this requirement, such as a BJT connected antiparallel with a diode, but these switches will have different electrical characteristics. Also unlike the previous mentioned switches, the MOSFET has an oxide layer between the p-type and n-type semiconductor materials, preventing unwanted conduction between the gate terminal and the semiconductor terminals.

The MOSFET is a three-terminal device. Current flows between the source and drain terminals when the device is ON, and the voltage at the gate terminal controls this current flow. When a positive drain-source voltage is present and a gate-source voltage below the threshold voltage level of the device is applied, the device operates in its OFF mode, where ideally no current flows between the drain and source terminals. However, when a positive drain-source voltage is present and a gate-source voltage above the device's threshold voltage value is applied, an electric field is created pointing away from the gate and across the p-region directly under the gate [31]. This electric

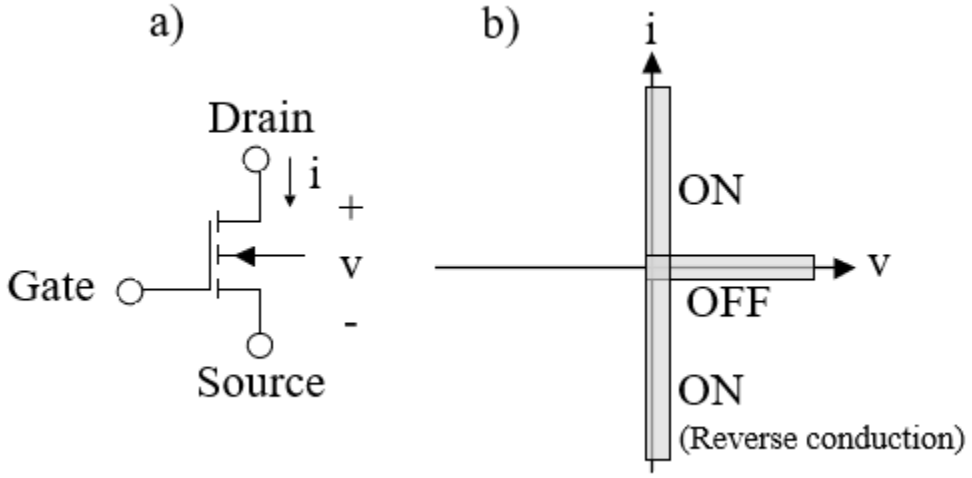

Figure 2.4: The symbol (a) and characteristics (b) of a MOSFET [12]

field causes the holes in the p-type body of the MOSFET to move away from the gate, creating an n-channel of charge in its place. By increasing the gate voltage, the size of the n-channel is increased, allowing more current to flow between the drain and source terminals. When a substantial amount of current is flowing from the drain to the source terminal, the device is considered ON.

Like the other devices mentioned, there are many variations of the MOSFET, but for higher power applications (typically up to a few kilowatts), the power MOSFET is utilized. One of the more common types of power MOSFET is the vertically-diffused MOSFET (VDMOS) shown in figure 2.6.

Unlike the BJT, the MOSFET is driven by voltage rather than current. Due to the MOSFET's high input impedance, the device's input current and power dissipation are reduced, allowing its gate drive circuitry to be relatively simple. MOSFETs exhibit very high switching speeds compared to other semiconductor devices. These advantages, along with the MOSFET's ruggedness and ease of application, have made it the dominant device used in lower power applications.

2.1.4 IGBT

The next semiconductor switching device to be discussed is the insulated gate bipolar transistor (IGBT). The IGBT combines the characteristics of a MOSFET and a BJT in a Darlington-type configuration, as shown in figure 2.7 [11]. This configuration allows the IGBT to take advantage of

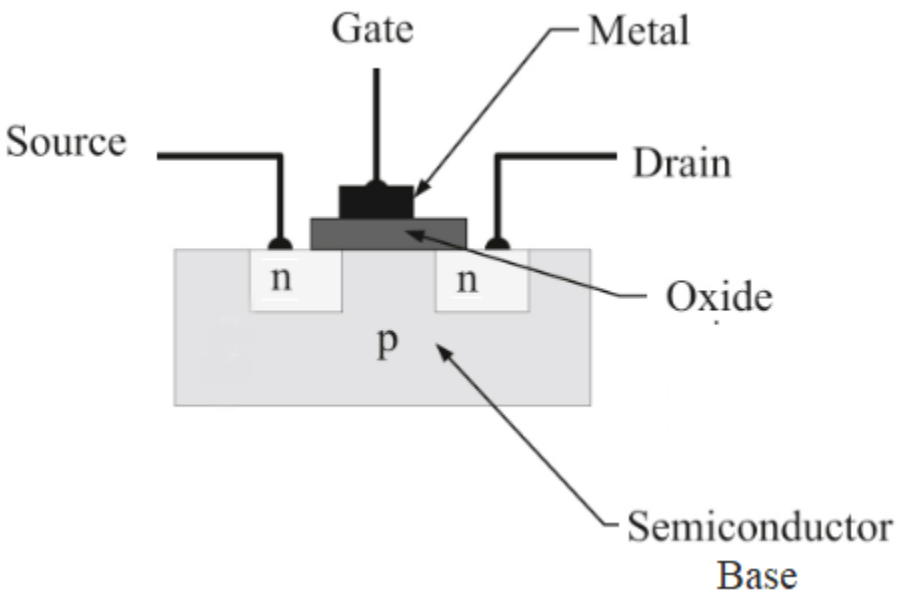

Figure 2.5: The cross-sectional view of a MOSFET [31]

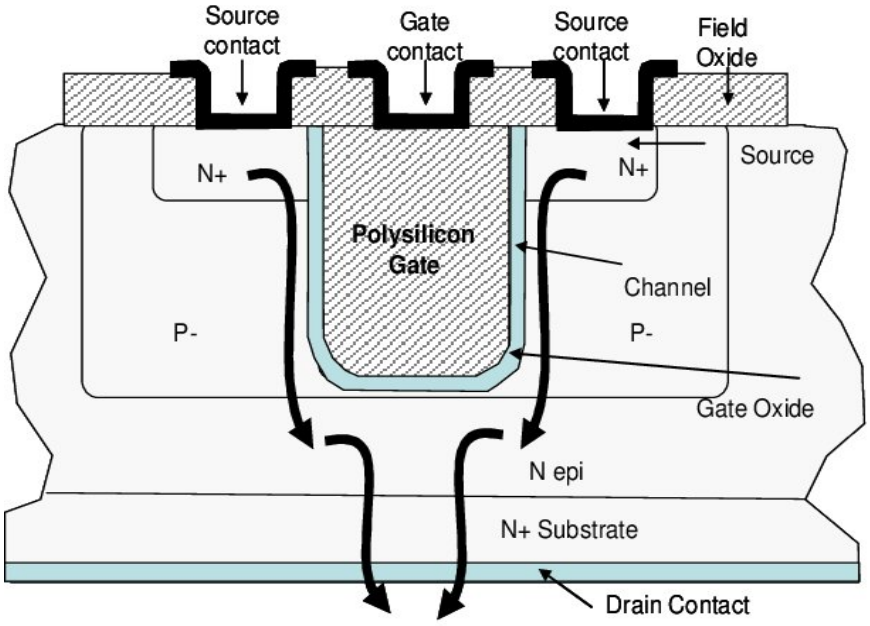

Figure 2.6: The cross-sectional view of a VDMOS device [18]

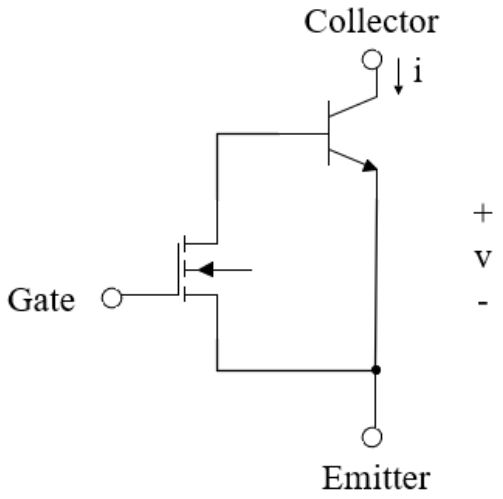

Figure 2.7: The IGBT's equivalent Darlington configuration of a MOSFET and BJT

the high switching speed and high input impedance of the MOSFET, along with the high current handling capability of the BJT. Similar to the previously mentioned devices, the IGBT is constructed from n-type and p-type semiconductor layers, as depicted in figure 2.8. In this figure, J_1, J_2, and J_3 represent the p-n junctions that the current encounters as it flows from the collector terminal to the emitter terminal of the device. The IGBT also facilitates vertical current flow, similar to the power MOSFET, so that the current-carrying area is maximized.

Like the MOSFET, the IGBT is a three-terminal voltage-controlled device. Applying a sufficient voltage to its gate terminal allows current to flow between the collector and emitter terminals, placing the device in its ON state. In the absence of gate voltage, ideally no current should flow, rendering the device in its OFF state. The symbol and characteristics of the IGBT are shown in figure 2.9. However, unlike the MOSFET, the IGBT can only conduct current of one polarity. Therefore, in AC applications where current of both polarities is required, the IGBT must be connected in antiparallel with a diode. This arrangement allows the device to exhibit the same ideal IV characteristics as the MOSFET.

Although the IGBT combines features of both the MOSFET and BJT, it has its own set of advantages and disadvantages compared to each individual device. The IGBT offers higher current gain and faster switching speeds than a standalone BJT. Additionally, due to its voltage-controlled operation, the driving circuitry required for the IGBT is simpler than that of the BJT. In comparison to the MOSFET, the IGBT exhibits lower power losses and higher power handling

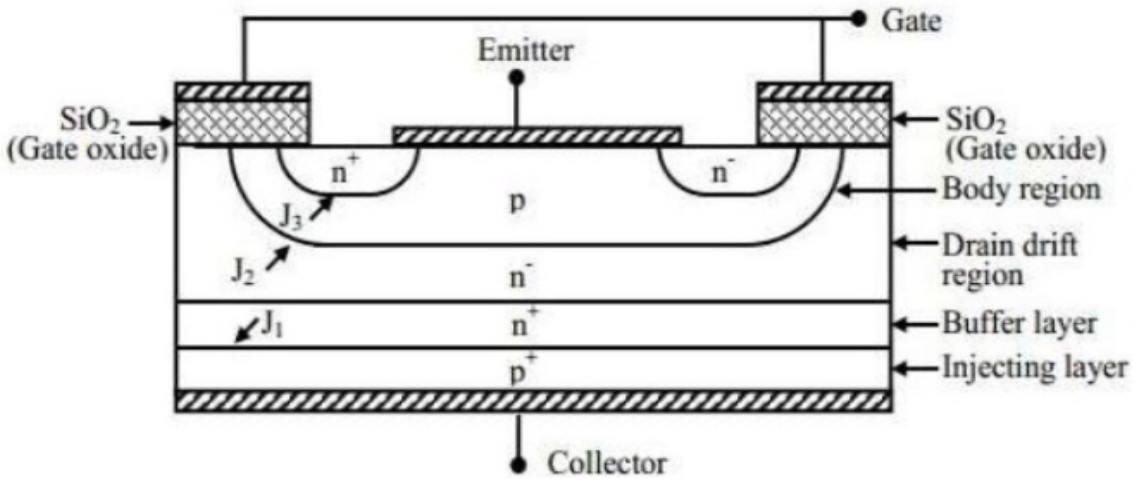

Figure 2.8: The cross-sectional view of an IGBT [10]

capability. However, it is important to consider the disadvantages as well, one disadvantage being slower switching speeds compared to the MOSFET. In addition, there is increased cost as well as are more failure mechanisms for the IGBT compared to standalone BJT or MOSFET devices.

Due to its higher cost and lower switching speeds, the IGBT is less commonly used compared to the MOSFET in lower power ranges. Additionally, since the BJT is also less expensive, the IGBT may not be the preferred choice for high-power applications that require low switching frequencies. Typically, the IGBT finds its niche in high-power and high-frequency applications. Some examples of its abundant applications in this range include industrial motor drives, aerospace electronics, electric cars and trains, and air conditioners.

2.2 Converter Losses

Ideally, designers strive for switches with zero ON-resistance that can operate either fully turned ON or fully turned OFF. In such ideal conditions, switches would exhibit no power losses, resulting in a converter efficiency approaching 100%. However, achieving these conditions is impossible in practical scenarios. As a result, power losses are inherent in power converter switches. This section focuses on the primary types of power losses associated with power converter switches, specifically analyzing the power losses related to using an IGBT with an antiparalleled diode as a switch. This choice of switch is relevant as it is utilized in the simulations presented later in this

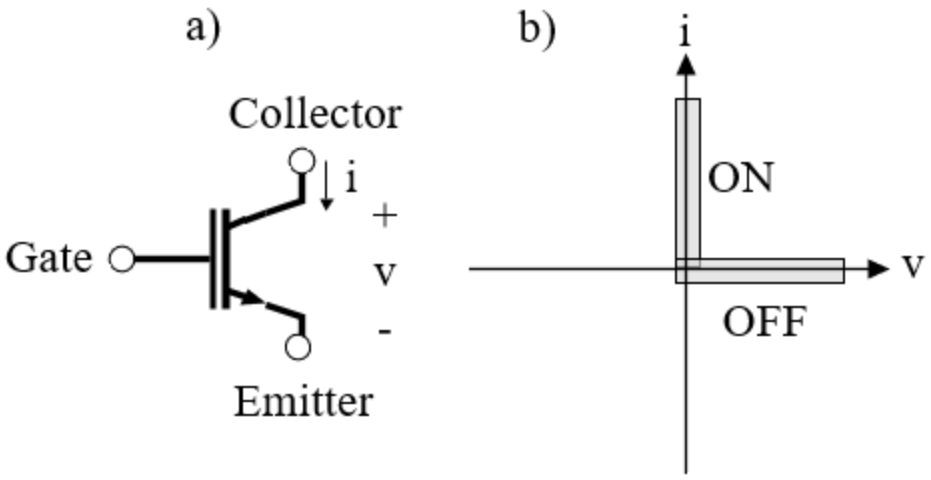

Figure 2.9: The symbol (a) and characteristics (b) of an IGBT [12]

thesis.

One of the two dominant power losses associated with a converter's semiconductor switches is conduction loss. When a switch is turned ON, it does not have infinite conductivity, leading to conduction loss. Similarly, when a switch is turned OFF, it does not have infinite resistivity, leading to blocking loss. Consequently, when a switch is placed in an active circuit, there is always some amount of current flowing through it. This current encounters a resistance component associated with the switch. And according to Ohm's Law, a voltage drop occurs across the switch. By multiplying the voltage across a switch by the current flowing through it during either the ON or OFF state, the conduction or blocking loss can be calculated. However because the blocking loss is so small is it typically not included in power loss calculation. But the conduction losses of an IGBT and diode can be easily determined as follows:

$$P_{cond,IGBT} = V_{CE(Sat)} \bullet I_C \tag{2.1}$$

$$P_{cond,D} = V_F \bullet I_F \tag{2.2}$$

where $V_{CE(Sat)}$ and I_C represent the voltage across the collector-emitter terminals of the IGBT and the current flowing through the IGBT when the IGBT is turned ON, while V_F and I_F are the voltage across the diode terminals and the current flowing through the diode when the diode is turned on,

respectfully.

The other dominant power loss associated with a converter's semiconductor switches is switching loss. Switching loss occurs when a semiconductor device transitions between its ON-state and OFF-state modes. These devices are unable to switch instantaneously between the two states. As a result, during the transition, a significant current flows through the device while a significant voltage exists across the device terminals. The speed of this transition depends on the type and size of the semiconductor device. The quicker the switching speed of a device, the lesser the amount of switching loss the device will experience. However, in applications that involve frequent switching transitions, the cumulative effect of this small loss becomes significant, making switching loss a critical factor that ultimately determines the maximum operating frequency of a converter.

To calculate switching loss, designers must use information such as the ON-state and OFF-state switching energy loss of a device provided in the manufacturer's manual. Using this information, the switching energy loss of an IGBT and diode can be calculated as:

$$E_{sw,IGBT} = (E_{ON} + E_{OFF})\left(\frac{I_C}{I_{ref}}\right)^{K_{i,IGBT}} \left(\frac{V_{DC}}{V_{ref}}\right)^{K_{v,IGBT}} \Big(1 + TC_{sw,IGBT}(T_{j,IGBT} - T_{j,IGBT,ref})\Big) \tag{2.3}$$

$$E_{sw,D} = E_{rr}\left(\frac{I_F}{I_{ref}}\right)^{K_{i,D}} \left(\frac{V_F}{V_{ref}}\right)^{K_{v,D}} \Big(1 + TC_{sw,D}(T_{j,D} - T_{j,D,ref})\Big) \tag{2.4}$$

where E_{ON} and E_{OFF} are the turn ON and turn OFF energy losses of an IGBT and E_{rr} is the diode recovery energy. I_{ref} and V_{ref} are the reference values for the current and voltage used in the datasheet for the switching loss measurements of each respective device. $T_{j,IGBT,ref}$ and $T_{j,D,ref}$ are the reference junction temperatures of the IGBT and diode that are used in the datasheet for switching loss measurements. $K_{i,IGBT}$, $K_{i,D}$, $K_{v,IGBT}$, $K_{v,D}$, $TC_{sw,IGBT}$, $TC_{sw,IGBT}$, $TC_{sw,D}$ are constants that can be obtained from the manufacturer's datasheet using curve fitting techniques[56]. However, due to the innate behavior of IGBT devices and diodes, these constants can be approximated in order to obtain adequate results for power loss calculations. $K_{i,IGBT}$ and $K_{i,D}$ can be respectively approximated as 1 and 0.55, $K_{v,IGBT}$ and $K_{v,D}$ can be respectively approximated as 1.3 and 0.6, and $TC_{sw,IGBT}$ and $TC_{sw,D}$ can be respectively approximated as 0.003 and 0.0055 [56].

After calculating the switching energies, the total switching losses for a switching period can

be determined by multiplying the switching frequency f_{sw} with the sum of the switching energies for the IGBT and diode, as shown in equation 2.5. The total conduction losses can be obtained by adding the conduction losses of the IGBT and diode, as shown in equation 2.6.

$$P_{sw} = f_{sw} \cdot (E_{sw,IGBT} + E_{sw,D}) \tag{2.5}$$

$$P_{cond} = P_{cond,IGBT} + P_{cond,D} \tag{2.6}$$

Once the total switching losses and conduction losses have been determined for each switching period, the total losses can be calculated using equation 2.7:

$$P_{loss} = P_{sw} + P_{cond} \tag{2.7}$$

It is important to note that the equations presented for conduction and switching losses provide close approximations that work well for mathematical models. These equations do not yield exact results as they do not account for variables such as device degradation and parasitic inductances, which can influence power loss. Despite these factors being present in devices, their impact is usually insignificant enough to be excluded from the equations. Also, while conduction and switching losses are the main losses associated with switching converters, there are other losses such as the previously mentioned blocking loss. And these losses are typically negligible as they do not significantly affect mathematical models, making their inclusion unwarranted due to increased model complexity.

2.3 Switch Materials and Performance

Material selection is imperative in the design of power electronic devices, as the material significantly influences device performance and efficiency. The properties of materials used in switching devices directly impact power losses. Therefore it is essential to understand how different material properties affect performance in order to optimize the design of power electronic devices.

Most of the semiconductor devices in today's world are made of silicon. This is because silicon is an element that not only allows for both adequate conduction and blocking of electricity, but silicon is also cheap to obtain as it is the second most abundant element in the Earth's crust,

accounting for about 27.7% of the Earth's crust by mass [37]. Although silicon devices works well, especially at low voltage ranges, there has been more research into the use of wide bandgap (WBG) devices for applications that require high-power and high-frequency switching.

The bandgap is the energy difference between the valence band and the conduction band in a material. It represents the amount of energy required for electrons to conduct in a material. Metals have no bandgap, resulting in high conductivity, while insulators have a large bandgap, resulting in minimal conductivity. Semiconductors have bandgaps that fall in between, providing them with semiconductive properties. The bandgap energy of silicon is 1.12 electron-volts (eV). While there is no definitive value for the bandgap energy of WBG semiconductors, it typically ranges from 2 to 4 eV [53].

Due to over 60 years of research and development, silicon-based power devices are now approaching their theoretical limits [50]. These material limitations hamper the electrical and thermal performance improvements of switching converters. As a result, silicon-based devices face challenges in meeting the increasing demands for higher efficiency, control bandwidth, power density, and switching frequency required by applications such as hybrid/electric vehicles, solar and wind energy systems, industrial automation systems, and smart grids [17]. Consequently, many researchers have shifted their attention to WBG devices. Two prominent WBG materials for high-voltage, high-power (600V, 1kW) applications are gallium nitride (GaN) and silicon carbide (SiC) [58].

Table 2.10 presents some of the essential physical properties of silicon (Si), GaN, and SiC [17]. It is important to note that the values of these properties may vary in different literature sources due to factors such as growth methods, material purity, and temperature during property measurement [17, 51, 62]. Nonetheless, the table shows that the bandgaps of GaN and SiC are approximately three times larger than that of silicon. This directly results in significantly reduced power losses in the OFF-state of WBG devices [51]. While some leakage current still exists in the OFF-state, WBG materials require higher energy for electrons to transition from the valence band to the conduction band, leading to reduced leakage current. Moreover, the larger bandgap enables WBG devices to operate at higher temperatures and withstand greater radiation exposure compared to silicon-based materials [62]. This makes WBG devices suitable for aerospace applications. Combined with their higher thermal conductivity, WBG materials offer the potential for higher system ambient temperatures and relaxed cooling requirements for power systems [17].

Table 2.10 also shows that GaN and SiC have larger breakdown fields, allowing for thinner

Semiconductor Material	Bandgap [eV]	Breakdown Field [x10^6 V/cm]	Saturation Drift Velocity [x10^7 cm/s]	Mobility [cm^2/(Vs)]	Thermal Conductivity [W/(cm.°C)]
Si	1.12	0.3	1	1400	1.3
GaN	3.4	2.5	2.5	2000	1.5
SiC	3.27	3	2	900	4.9

Table 2.10: Physical Properties of Semiconductor Materials [17]

device structures than silicon-based devices while maintaining the same blocking voltage. Thinning a device reduces its ON-resistance, resulting in decreased conduction losses. Another significant material property in table 2.10 is the electron saturation drift velocity, which indicates a material's mobility under a high electric field. GaN and SiC exhibit double the electron saturation drift velocity compared to silicon, meaning that electrons in GaN and SiC can reach double the maximum velocity of electrons in silicon under high electric fields. This lower ON-resistance, coupled with higher electron velocities, makes WBG devices better suited for applications requiring high switching speeds. The larger electron saturation drift velocity of WBG materials leads to shorter switching times and reduced reverse recovery charge, resulting in lower switching losses [58, 19]. The decrease in switching losses enables higher switching frequencies, improving system control and allowing for smaller filtering components, facilitating miniaturization [17].

Although WBG devices offer significant advantages over conventional silicon-based devices, they currently account for less than 1% of the global semiconductor market [2]. Cost is one of the primary factors contributing to this situation. Because silicon is such an abundant material it is much cheaper to obtain than WBG materials. Reliability issues also hinder the dominance of WBG devices in the market. These issues stem from inherent challenges in the development of these devices. GaN devices, for instance, may have reliability issues related to defects in the material's crystalline lattice during growth [28]. SiC devices also face reliability issues associated with charge trapping in the oxide layer. These reliability problems can degrade device performance and cause operational instability. However, as WBG devices are relatively new, ongoing research will address these challenges, leading to improved device characteristics similar to those of first-generation and second-generation semiconductors.

Chapter 3

Electric Power Conversion

Electric power conversion is the process of transforming one form of electrical energy into another using a network of semiconductor switches, such as the ones discussed about in the previous chapter. This process is critical to virtually all areas of modern life, from power distribution and renewable energy systems to consumer electronics and hospital medical equipment [27, 55]. Power conversion involves controlling the switches in the network to transform the incoming power into a different, desired output power. There are four main categories of power conversion:

- AC-to-DC
- DC-to-AC
- DC-to-DC
- AC-to-AC

3.1 AC-to-DC Conversion

AC power, which periodically changes direction, needs to be converted into DC power, which flows in only one direction, for many consumer electronics to function. This process is known as AC-to-DC power conversion or power rectification. This conversion is necessary for many consumer devices because these devices typically require DC power to operate, but are sourced by the AC power available through the wall socket that is provided by utility companies. For simple consumer

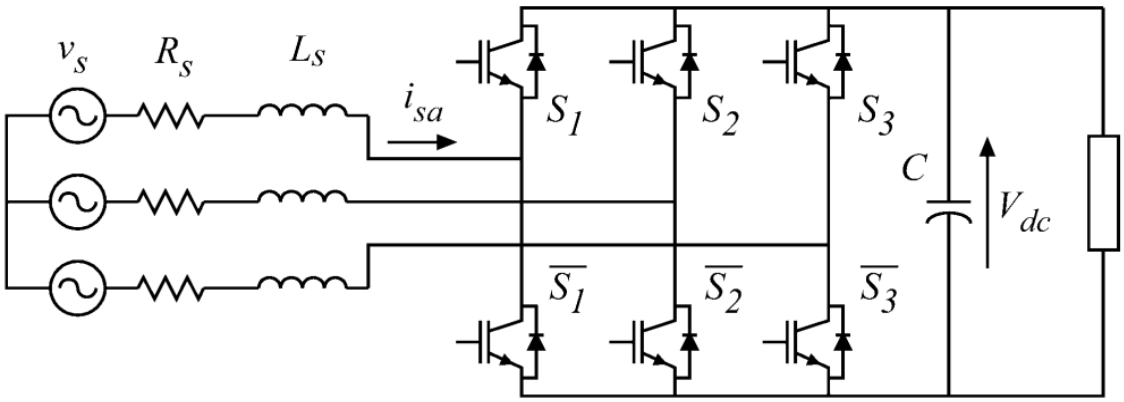

Figure 3.1: An active front end rectifier (AFE) [6]

devices, a single-phase full-wave rectifier is commonly used. However, for more complex and high-powered applications, such as industrial DC motor control, high-voltage DC transmission lines, and electric car battery charging systems, a more sophisticated, three-phase rectifier topology is required [27, 55]. One such topology, which is discussed in greater detail throughout this section and used for simulation in the later part of this thesis is the two-level, three-phase active front end rectifier (AFE).

Among the various types of two-level, three-phase rectifiers, the AFE stands out for its superior performance capabilities. As depicted in figure 3.1, each switch consists of a power device connected with an antiparallel freewheeling diode, which allows for full control and fast switching. The figure also shows that the AFE has an input inductive filter as well as its equivalent series resistance attached to every line of the rectifier. The filter is used to suppress high-frequency harmonics generated by the AFE from propagating back into the AC voltage source. There is also an output capacitive filter which helps to reduce the voltage ripple on the DC-link by filtering out high-frequency voltage components from the AFE. This helps to maintain a stable DC voltage and prevent voltage fluctuations. In contrast to other two-level, three-phase rectifiers such as diode or thyristor rectifiers, the AFE offers several advantages, including a highly controllable DC voltage, controlled input currents with reduced harmonics and sinusoidal waveform, unity power factor operation, and full regenerative operation [46].

An AFE functions as a boost converter during rectification, stepping up voltage from a minimum value, roughly equal to the peak value of the line-to-line supply voltage [55]. It is crucial

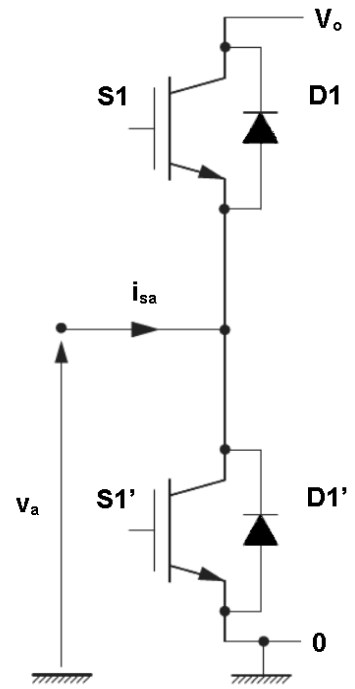

Figure 3.2: Phase-A leg of an active front end rectifier (AFE) [55]

to ensure that no complementary switches in a single branch are turned ON simultaneously, as this could short the DC-link capacitor with potentially dangerous current. Although ideal complementary pairs involve having one switch ON and the other OFF, practical scenarios may have brief periods where both switches are turned OFF due to non-ideal switch behavior. To avoid shorting the DC-link capacitor, designers introduce a "dead-time" between switching transitions where both switches are turned OFF. Taking a look at figure 3.2, it can be seen that if a pair of complementary switches are turned OFF at the same time, then depending upon the polarity of the input current i_{sa}, current would flow through either $D1$ or $D1'$ allowing the phase leg terminal voltage to equal either V_0 or 0, respectively [55].

3.2 DC-to-AC Conversion

DC-to-AC power conversion, also known as inversion, involves altering the direction of current flow from a singular direction in DC circuits to a periodically changing direction in AC circuits. Inverters are essential in critical facilities like hospitals, communication centers, airports,

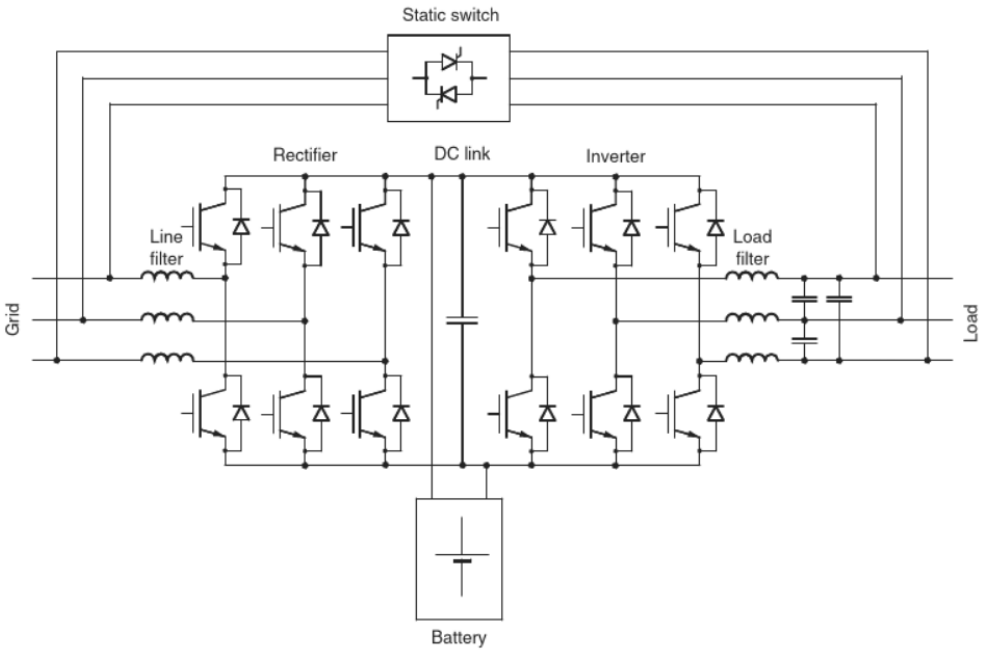

Figure 3.3: A basic uninterruptible power supply (UPS) system [55]

and military installations, where a constant and uninterrupted power supply is crucial [55]. These facilities often rely on their own uninterruptible power supply (UPS) system, as shown in figure 3.3, which charges up a backup battery from the grid using a rectifier [55]. In case of a power grid failure, the stored electric power in the battery is converted back to AC using an inverter, which can then supply the critical equipment that needs it.

As previously discussed, the AFE is a type of power converter that has full regenerative operation, allowing for bidirectional current flow. This feature makes the AFE a versatile power converter topology that can be used for not only rectification, but inversion as well in various medium and high-power industrial applications. Applications where the AFE is used for inversion include: induction motor drives, synchronous machine drives, and hydro and wind power plants [30]. The ability of the AFE to operate in both rectification and inversion modes makes it a popular choice for industrial applications where energy efficiency, high-power quality, and reduced harmonic distortion are essential.

3.3 AC-to-AC Conversion

AC-to-AC power conversion involves converting an AC signal with fixed magnitude and frequency into another AC signal with controlled amplitude and frequency [46]. Various circuit topologies can perform AC-to-AC conversion. Some circuits directly convert an AC signal to another AC signal, while others utilize a rectifier and DC link to convert and store the signal as DC, followed by an inverter to transform it back to AC. An example of this indirect conversion is the UPS system, where the output AC signal can have adjusted amplitude and frequency, albeit with a lower amplitude than the input signal.

Matrix converters are a direct type of AC-to-AC converter that utilizes bidirectional fully controlled switches and eliminates the need for a DC link capacitor present in indirect conversion methods. This allows for the possibility of circuit miniaturization. Matrix converters can adjust both the amplitude and frequency of the signal, although the output amplitude will be reduced compared to the input signal. Matrix converters have inherent limitations on their voltage gain (0.866) and require a more complex control and protection strategy [30]. While the limited voltage gain restricts matrix converter employment in AC motor control applications, these converters can be found in areas such as high-performance drives, wind-turbine systems, and electric and hybrid vehicles [55].

In another direct AC-to-AC conversion approach, cycloconverters can convert high-voltage and high-frequency AC source voltage to a variable, lower output voltage and frequency [30]. Cycloconverters are commonly used for controlling large AC motors, particularly synchronous motors, in low-speed, high-power drive systems like rolling mills and cement kilns [55]. The low output frequency of a cycloconverter allows for low motor speeds, facilitating direct gearless drive of the load. Additionally, cycloconverters enable rapid acceleration and deceleration and support regenerative operation over the entire speed range [55].

3.4 DC-to-DC Conversion

DC-to-DC conversion involves converting an input DC signal into a DC signal with a different amplitude. Among the numerous types of DC-to-DC converters, three fundamental topologies are commonly used: buck, boost, and buck-boost [30]. Buck converters step down the input DC signal to a desired value and operate in the first quadrant of the voltage-current plane. This means

they can only generate positive DC output voltage and current, with power flowing from the source to the load. On the other hand, boost converters step up the input DC signal to a desired value and operate in the second quadrant of the voltage-current plane. This results in a positive output voltage and a negative average output current, with power flowing from the load to the source. Buck-boost converters can both step down and step up the input DC signal, operating in the third quadrant of the voltage-current plane. This allows for bidirectional power flow between the load and source while maintaining a positive output current.

Chapter 4

Power Converter Control

After discussing power converter switches and electrical energy conversion, it is important to examine the techniques used to control power converter switches in order to achieve desired energy transformations. Without applying any control method to a converter's switches, the converter may operate erratically and even damage circuit components if the output power exceeds the exceeds that of rated components.

There are various switching methods available, each with its own advantages and limitations. The choice of method can have a profound impact on the performance and efficiency of a power converter. In this section,a few common control methods used in converters and their respective merits are discussed.

Regardless of the switching method used it can be classified into one of two groups: open-loop control and closed-loop control. Open-loop control operates without considering any measurements of the system, relying solely on predefined actions. For example, a soda fountain in a fast food restaurant uses open-loop control when a user presses a button to dispense a soft drink. The drink will continue to flow until the user manually stops it, as the appliance cannot monitor its output. Open-loop control is often preferred for its simplicity and cost-effectiveness. It eliminates the need for sensors to monitor system variables, saving both money and space. However, open-loop control has limitations, including sensitivity to input signal disturbances, inability to handle changing system parameters over time, and inability to stabilize initially unstable systems [24]. Therefore, open-loop control should only be used in stable systems with low levels of disturbance and uncertainty [24].

In contrast, closed-loop control incorporates system measurements and feeds them back into

a controller for more accurate and reliable operation. Cruise control systems in cars are a common example of closed-loop control. The driver sets a desired (reference) speed, and the system adjusts the throttle using feedback from a speed sensor to maintain the reference speed. If the car's speed deviates from the reference, the system adjusts the throttle accordingly. Closed-loop control is widely used in industrial applications to maintain steady-state operation and meet industrial requirements [30]. Closed-loop control offers several advantages over open-loop control, including the ability to respond to disturbances, parameter changes, and load uncertainties, as well as the capability to change system dynamics [24]. However, closed-loop control also has disadvantages, such as the additional space and cost required for sensors, measurement noise introduced by sensing equipment, and increased system complexity [24].

4.1 180° Voltage Source Operation

The first control method that will be discussed is 180° voltage source operation, also known as six-step operation. This is an open-loop control strategy that is typically employed in inverters. In a two-level, three-phase converter, 180° voltage source operation functions by allowing each switch in a converter leg to conduct for 180° out of every 360°electrical cycle. Ideally, no pair of complimentary switches should ever be turned ON or turned OFF at the same time. Also there is a 120° electrical separation maintained amongst each converter leg.

With this approach, a continuous current flow is maintained in each phase leg of the converter. 180° voltage source operation produces square wave voltages and currents for the load, rather than smooth sinusoidal waveforms. Consequently, these signals contain high amounts of harmonic content. To mitigate this harmonic content, appropriate converter filters must be selected. Failure to address the harmonic content can lead to various detrimental effects in a power system, including reduced power quality, equipment overloading, decreased system efficiency, reduced torque, and increased vibration and motor heating.

180° voltage source operation is sometimes used as a control method for inverters driving motors. This switching technique maximizes the inverter's capability while minimizing the switching frequency [21, 40, 36], resulting in enhanced torque compared to other control techniques.

4.2 Pulse Width Modulation

Pulse width modulation (PWM) is a control strategy that originated in telecommunications, and has since become a widely-used technique for controlling the power delivery in various converter topologies. PWM is valued for its high efficiency, flexibility, precise output control, and ease of implementation. That is why it can be found in a broad range of applications, from low-power device battery regulation systems to large-scale HVDC transmission systems [32, 8]. There are many different varieties of PWM, but one of its simplest forms is carrier-based sinusoidal pulse width modulation (SPWM). In carrier-based SPWM, output signals are constructed by comparing a carrier signal and a reference (or modulation) signal. The carrier signal is a high-frequency waveform, typically triangular or sawtooth in nature. The modulation signal can be any shape, however, in the case of SPWM, the modulation signal is that of a sine wave. In the case of an inverter, the output voltage of a phase leg is determined by comparing the instantaneous magnitude of the modulation signal with that of the carrier signal at a point in time. If the modulation signal is greater than the carrier signal, the output voltage of the inverter leg should be connected to the positive side of the DC link. This corresponds to a positive voltage on the load. On the other hand, if the modulation signal is less than the carrier signal, the output voltage should be connected to the negative side of the DC link, which corresponds to a negative voltage on the load [26]. Correspondingly, the pulses sent as control inputs to the semiconductor switches have varied widths in order to control the amount of power delivered to the load. The duty cycle of the PWM waveform, which is the ratio of the pulse width to the period of the carrier wave, determines the average power delivered to the load. By adjusting the duty cycle of the PWM waveform, the amount of power delivered to the load can be varied in a precise and efficient manner [1].

Because of the abrupt changes between the high and low states generated by PWM, there are a lot of high-frequency components being added to the signals fed to the converter switches, reducing the switching device efficiency. As a result, there is much research on eliminating unwanted harmonics through enhanced PWM techniques such as using a modified carrier signal instead of a conventional triangular or sawtooth signals [1]. Research also extensively explores using closed-loop PWM control for force-commutated, three-phase voltage source rectifiers, which can meet various industrial requirements such as power factor correction, harmonic elimination, regenerative traction power supplies, frequency link conversion, and four-quadrant operation [8].

4.3 Finite Control Set Model Predictive Control

Model predictive control (MPC) is an advanced form of control that can be used for modulation, although it is not specifically a modulation technique. MPC has been around since the 1970s but was not feasible for systems that required millisecond response times until the 1980s [48]. This is because of the heavy computational burden required by MPC algorithms could not be solved quick enough to be utilized in power electronics until the development of microprocessors and computer processing abilities. MPC employs a dynamic model to predict the future behavior of a plant. By utilizing this predictive information and minimizing a cost function, it determines the optimal input required to achieve the desired reference [48]. The plant is often modeled using transfer functions or state space equations.

MPC offer several advantages over conventional linear control methods, such as previously mentioned 180° voltage source operation and PWM, due to its predictive capabilities. These advantages include better handling of: decision-making involving approaching constraints, interactions with multi-input-multi-output (MIMO) systems, future variations and disturbances, and system dynamics such as delays [47]. While linear control methods can address these issues, it is done in a tentative manner and can bring about unpolished results due to non-linearity or instability, rendering the system models invalid. Other benefits of MPC include its design simplicity, flexibility to operate in various conditions and environments, ability to control multiple objectives while satisfying multiple constraints, and potential for modification to provide a modular control scheme [47].

One commonly used specification of MPC employed in the field of power electronics is finite control set model predictive control (FCSMPC). FCSMPC enables current tracking and eliminates the need for intermediate modulation processes. In power electronics control, FCSMPC predicts the future behavior of a power system over a predefined time horizon. By considering the power converter's finite number of possible states (or switching positions) and taking into account its current and past states, FCSMPC determines the next optimal state to satisfy the chosen optimization criteria, which is quantified by the cost function [23]. The selected state is directly applied at the next sampling instant, and the algorithm repeats its calculations using the updated system conditions to determine the required switching actions in subsequent sampling instants for optimal system operation. The complexity of the discretized system equation increases the potential for more desirable system behavior. But it is important to note that at some point, excess effort spent

on system accuracy brings diminishing returns as the extra time and money costs will eventually result in very little impact on system behavior. So, it is of common understanding that the model used in accordance with FCSMPC should be "fit for purpose" which is where the model generates the required results to a necessary level of accuracy within a manageable amount of time [60].

Unlike the previously mentioned linear control techniques, FCSMPC does not provide a fixed switching frequency, as switching may not be required during every sampling period based on the algorithm's calculations. However, an average switching frequency can be determined, representing the average number of switching actions of a single converter per second. Similar to other modulation schemes, a higher average switching frequency results in increased switching losses. Nonetheless, it is important to keep in mind that the additional switching losses are the cost for the opportunity to miniaturize filter components, allowing for greater power density in power systems.

FCSMPC predicts the future behavior of the system through a discretized equation of the general form [48]:

$$x(k+1) = Ax(k) + Bu(k) \tag{4.1}$$

where $u(k)$ is the system input vector, $x(k)$ is the state vector at the current sample time T, $x(k+1)$ is the state vector at the subsequent time sample, A is the state matrix, and B is the input matrix. The system input vector variables are manipulated by the algorithm in order to control the system. The state vector variables describe the system dynamics and typically includes any capacitor voltage(s) and/or inductor current(s).

Another important equation to consider is the cost function. The cost function is what the FCSMPC algorithm must minimize in order to optimize the system according to the user's requirements. Because the cost function quantifies the system optimization, it is also frequently referred to as the performance index. The cost function can have a single objective or multiple objectives. Although there is a general cost function associated with MPC, this can be simplified for FCSMPC. A two objective cost function used in FCSMPC can have the general form:

$$\epsilon = [x^*(k+1) - x(k+1)]^2 + [y^*(k+1) - y(k+1)]^2 \tag{4.2}$$

where ϵ is the error, k is the current discrete time, x* and y* are the reference signals used to calculate predicted behavior, and x and y are the corresponding signals being predicted. From equation 4.2, it can be seen that the cost function is essentially a quadratic error calculation. Although there are

various ways to compute the cost function, some methods involve maximizing the cost function for optimal performance rather than minimizing it. In [45], the authors explore different cost function calculations and discuss how they affect system performance. Weighting factors may be necessary in a system with multiple cost functions to satisfy a set of constraints. These factors quantify the importance of each cost function to the system. Without weighing factors, a system may not meet all system constraints as expected by the designer.

Chapter 5

Converter Thermal Management

Power electronic applications increasingly demand power converters that are compact, have high-power density, and operate at high switching frequencies. However, these requirements generate significant heat energy from the semiconductor switches. This heat energy can negatively impact the overall system performance and increase costs. Hence, it is crucial for designers to address thermal issues in power converters. This chapter will explore common heat energy problems that occur in converters and discuss active thermal management strategies that can mitigate these issues.

5.1 Thermal Issues in Converters

As discussed in chapter 2, each semiconductor device experiences power losses that are dissipated as heat energy. This heat energy leads to increased device energy loss and therefore system performance declines. The relationship between a converter's efficiency and heat energy is evident from the device switching loss equations covered earlier. Higher dissipated heat energy increases the junction temperature of switching devices, resulting in greater energy losses (as indicated by equations 2.3 and 2.4) and reduced efficiency.

Dissipated heat energy not only affects device power losses, but also device lifetime and reliability. According to Fabis et al. [15] as cited in Yuan et al. [63], temperature effects account for almost 60% of failures in IGBT modules. For every 10°C temperature rise of the junction temperature, the failure rate nearly doubles. The most common reason for module failure is due to thermomechanical stresses on the packaging materials [43]. These stresses occur due to a mismatch

in the coefficients of thermal expansion (CTE) between different adjacent materials inside the power module package, which increases with temperature [16]. Temperature swings caused by power cycling and thermal cycling contribute to these thermomechanical stresses. Power cycling refers to temperature variations caused by varying power loss in the devices due to a variation of operating conditions, while thermal cycling is the effect of temperature variations in the environment around the power module [43]. These stresses combined with device operation at excessive temperatures beyond device ratings, typically around 150°C for silicon IGBT modules, significantly reduce device lifetime and reliability [3].

5.2 Active Thermal Management

Various types of cooling methods can be employed to relieve heat energy from a converter. Using active cooling methods, such as forced-air cooling or liquid cooling, to dissipate heat energy in power electronic systems can increase a system's size, cost, reliability, and complexity. This can ultimately limit the achievable power density. Other methods of active thermal management (ATM), active thermal control (ATC) in particular, offer more effective solutions to alleviate heat energy without incurring the drawbacks associated with active cooling methods. ATC is a type of ATM, but the two phrases are often used synonymously. In this thesis, the only types of ATM that will be discussed are those considered as ATC.

ATM is used to control semiconductor module junction temperatures using a control parameter such as switching frequency, modulation method, DC-link voltage, device gate voltage, or circulating reactive power [16]. This technique incorporates thermal-related control parameters to improve the lifetime, reliability, and efficiency of the switching devices in a module. ATM often reduces thermal stresses by reducing temperature variations or the maximum thermal temperature allowed during transients and/or steady state. To minimize system costs and space utilization, thermal parameters can be estimated in some cases rather than relying on sensor readings, as long as the estimations are sufficient.

In order to achieve ATM, the simulations presented in this thesis control the switching frequency using temperature estimations based on device power losses. To accurately model the thermal behavior of the system, it is important to understand how the thermal model is developed. The following sections will discuss the development of a power loss model and a Cauer thermal

network model, which are essential components in achieving effective active thermal management.

5.2.1 Power Loss Modeling

The direction of current flow affects which device experiences switching losses, whether it's the upper IGBT or diode, or the lower IGBT or diode. This aspect was not discussed in detail in chapter 2 due to the lack of information on the rectifier topology, which was presented in chapter 3. As mentioned earlier, the proposed ATM system in this thesis will adjust the switching frequency to achieve lower device temperatures. However, it's important to consider the costs associated with switching in each device. Therefore, this subsection will discuss the effects of switching action and current flow direction on switching losses and how the model predictive control of the ATM system will evaluate these costs.

The affect of current flow and switching action can be seen by taking a look back at figure 3.2 where a single converter leg is shown. For conduction losses, it is simple to tell which device experiences loss as it is simply the device powered ON. But for switching losses, the switching action and current flow direction must be taken into account.

In a switching bridge, current flow is considered positive when it enters the phase leg, as illustrated in figure 3.2. To allow current to exit through the top switch, the upper diode must conduct, while the upper IGBT and the lower two semiconductors remain in the OFF state. If current needs to exit through the bottom switch, the lower IGBT conducts, while the other three semiconductor devices remain in the OFF state. This methodology for current flow direction and switching state also applies to the other legs of the converter, not just the A-phase. Conversely, when current leaves the phase leg, it is considered negative, and the opposite applies. For a negative current to exit through the top switch, the upper IGBT conducts, and its freewheeling diode and the lower two semiconductors remain in the OFF state. Similarly, if a negative current needs to exit through the bottom switch, the lower diode conducts, while the other three semiconductor devices remain in the OFF state. Table 5.1 shows the IGBT and diode currents according to the switching state, which corresponds to the current flow direction shown in figure 3.2 and described in this paragraph [38].

S1 State	S1' State	Current Direction	S1 Current	S1' Current	D1 Current	D1' Current
ON	OFF	$i_{sa} > 0$	0	0	i_{sa}	0
ON	OFF	$i_{sa} < 0$	i_{sa}	0	0	0
OFF	ON	$i_{sa} > 0$	0	i_{sa}	0	0
OFF	ON	$i_{sa} < 0$	0	0	0	i_{sa}

Table 5.1: IGBT and diode currents according to the switching states [38]

5.2.2 Cauer Thermal Network Modeling

In regards to achieving ATM for a converter, there needs to be a thermal model of the converter itself. Modeling the junction temperature deviation of semiconductor devices in real-time is a challenging task, because the physical behavior is based on the three-dimensional heat transfer and there is a high degree of thermal coupling as the heat from one device can cause additional heating in adjacent devices [38]. One way to model a system is through finite element analysis (FEA). FEA can be used to analyze three-dimensional heat transfer, but it requires proprietary information about a power module's makeup that is not provided by the manufacturer [39]. In addition to this, FEA is not suitable for real-time implementation in power electronics due to its high computational power requirements and high-order modeling. While modeling the junction temperature deviation of semiconductor devices in real-time is challenging due to the complexity of three-dimensional heat transfer and the lack of proprietary information, alternative techniques such as a lumped parameter model can be used to achieve ATM. This simplified model represents a single path of heat propagation from the semiconductor device junction to the heatsink and can be implemented in real-time without the high computational power requirements of FEA.

The Cauer thermal network, depicted in Figure 5.2 [39], is a commonly used lumped-sum model in power converter analysis. It represents the converter's thermal behavior using voltage as temperature, current as heat flow, resistance as thermal resistance, and capacitance as thermal capacitance. Thermal resistances, R_{th}, and thermal capacitances, C_{th}, are obtained from the manufacturer's datasheet. Power loss, P_{loss}, and the ambient temperature, T_c, are the only inputs, however, the ambient temperature changes slowly and so it is often kept as a constant. The most crucial variable of interest is the junction temperature, T_j or x_1, as this is the temperature pri-

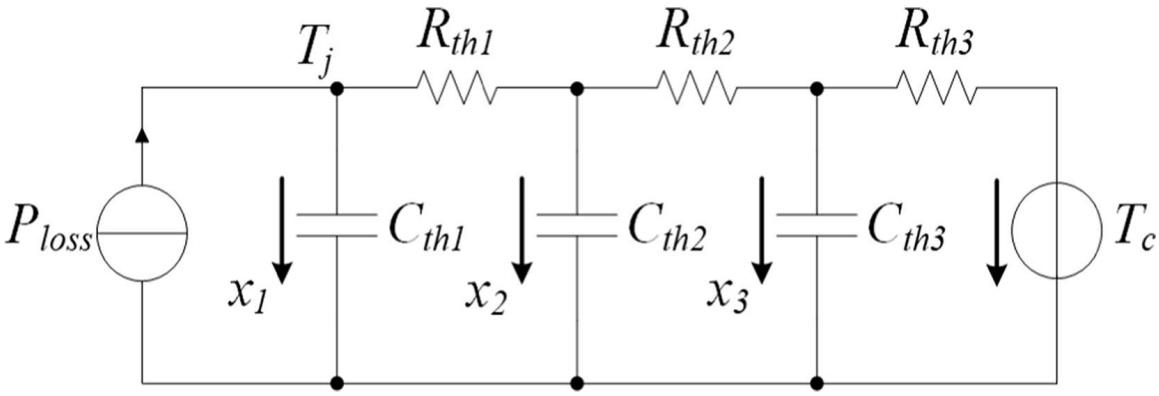

Figure 5.2: A third-order Cauer thermal network [39]

marily responsible for influencing the semiconductor device's operational behavior. By utilizing the Cauer network, approximate temperatures for each layer of the converter can be estimated, with the node voltages serving as representations. However, it is important to keep in mind that the network simplifies the three-dimensional heat transfer, leading to some degree of error in temperature prediction.

Chapter 6

Converters in Parallel

One IGBT module is sometimes not enough to handle a certain amount of power that a system requires it to handle. Instead of using a larger and/or a more expensive IGBT module that can handle higher amounts of power, one practical solution is to use multiple converters in parallel to handle the power. This allows for the use of smaller sized filters, allowing for system miniaturization. In addition, a modular scaling approach is enabled, allowing for expandability and a high degree of flexibility in power system design by easily integrating IGBT modules until the system's power handling needs are satisfied [44]. But not only does parallel operation of power converters offer the ability of increased power handling capacity and modularity, but it also can offer improved efficiency, enhanced reliability, and reduced output current harmonics [44, 54, 64].

When converters are paralleled, the current sent to the load is shared amongst the converters causing each converter to handle a smaller amount of current compared to a solo operating converter. Because each converter operates at a lower current level, thermal stress on each converter's components is reduced. This reduction in thermal stress helps mitigate additional power losses, allowing each converter to operate within its rated current range more efficiently. In addition, using multiple converters instead of a single converter will spread dissipated heat across a larger area further increasing the lifetime and reliability of semiconductor devices.

Paralleling converters can also provide redundancy, further strengthening system reliability [35]. If one converter fails, faults, or requires maintenance, the other paralleled converters can continue to supply power (albeit at a now higher current output) in order to avoid an entire system shutdown [5]. This is imperative to applications where a continuous supply of power is required.

6.1 Current Imbalance & Zero Sequence Current

While paralleling converters can offer numerous benefits over using a single converter, it is crucial to address potential drawbacks, such as imbalanced current flow between the converters. Any asymmetry in device or converter design can result in uneven current distribution. These asymmetries encompass factors like drive voltages, control signals, and device characteristics such as input impedance, threshold voltage, and switch turn ON and turn OFF times [22, 29]. Even when using identical converters from the same manufacturer, some level of asymmetry is inevitable. It is also important to note plenty of other system-level factors can also play a role in imbalanced current flow as well such as unbalanced sources and loads.

Current imbalance can significantly impact the performance of parallel operated converters. The converter with a higher current flow experiences increased thermal stresses on its components compared to the other converters in parallel. This excessive heat can lead to reduced reliability, lifetime, and overall performance. To address current imbalance, various control techniques and strategies have been developed, with many falling under the category of master-slave current sharing control or droop control [49]. However, in this thesis, the current imbalance issue will be mitigated through the implementation of a model predictive control algorithm, as elaborated in the simulation section.

The same factors that cause current imbalance, such as differences in hardware parameters and switching actions, can also result in the generation of a zero-sequence circulating current (ZSCC) as shown in figure 6.1 [61]. Variations in hardware characteristics and the asynchronicity of the switching actions among the paralleled converters give rise to a zero-sequence voltage which rapidly affects the equivalent resistance between the converters, leading to the formation of ZSCC [20].

Because ZSCC represents an undesired flow of current in a system, it is associated with various system performance limitations. It can distort the output currents of each converter, increase current stresses and conduction losses on semiconductor switches, increase the risk of converter failures and shutdowns, lower system efficiency, and potentially lead to system damage [44, 59]. Minimizing the magnitude of the ZSCC is essential to ensure optimal performance and reliability in parallel converter systems.

As ZSCC plays a significant role in overall system efficiency, researchers have developed various techniques to suppress it. One technique to suppress it is the use of high impedance current-

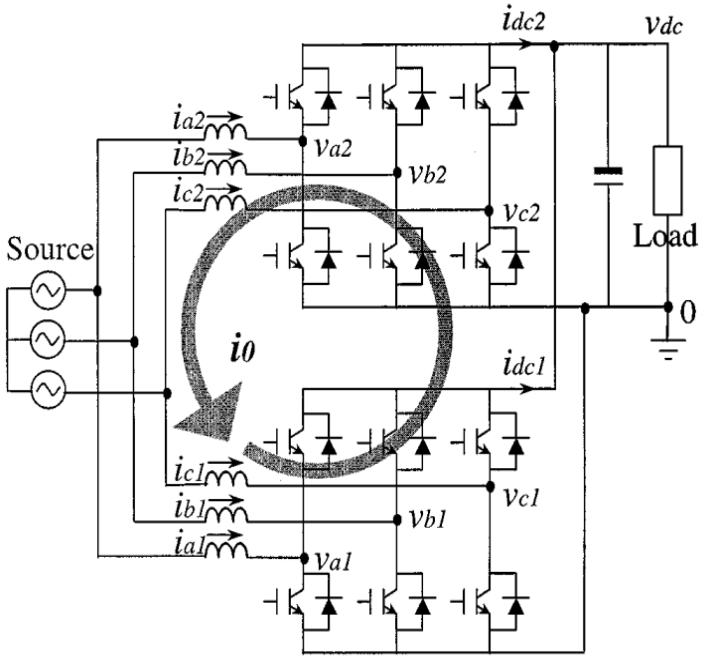

Figure 6.1: The circulating zero-sequence current in two directly paralleled active front end rectifiers [61]

sharing reactors [33]. This method effectively suppresses ZSCC at medium and high frequencies, however, it may not be as effective at lower frequencies. Therefore, additional methods should be considered to achieve ZSCC suppression across a wide frequency range, ensuring optimal performance of the parallel converter system.

An alternative and widely regarded technique to eliminate ZSCC involves isolation, where separate AC or DC power supplies are employed, providing a physical separation between the converters to mitigate ZSCC [25]. Another conventional method involves the use of an isolation transformer on the AC side, effectively transforming the ZSCC into an open circuit [9]. It is important to note that these isolation techniques often result in increased system bulkiness and cost, making alternative control-focused techniques more appealing.

A plethora of control techniques, particularly those involving PWM, have been employed to address the elimination of ZSCC in parallel converter systems [42, 59]. However, considering the advantages of MPC, as discussed earlier in this thesis, a centralized approach utilizing MPC is utilized in the simulations presented later in this thesis. While control techniques can adopt either a centralized or decentralized approach, decentralized control offers benefits such as speed, adaptability, and

redundancy. However, it can introduce many issue in implementation and coordination, potentially leading to increased ZSCC. As a result, to ensure an effective control strategy, the simulations in this thesis use a centralized approach, specifically focusing on synchronized control of the paralleled converters.

Synchronized control treats all the paralleled converters as a single control system, aiming to achieve coordination and optimized performance. However, it is important to note that synchronized control becomes increasingly complex as the number of paralleled converters increases, requiring careful consideration of system design in order to manage the added complexity.

Chapter 7

Control Algorithm Derivation and Validation

This chapter focuses on the simulations conducted to validate the performance of a control algorithm in a system consisting of two paralleled converters. The simulations aim to achieve three key objectives: stable regulation of the DC-bus voltage across the load, effective suppression of ZSCC, and implementation of ATM to mitigate device junction temperatures and eliminate thermal imbalance amongst converter switches. To accomplish these objectives, a comprehensive control model is developed, encompassing voltage regulation, ZSCC suppression, and an ATM strategy. The control algorithm is designed based on the proposed model, and its effectiveness is subsequently validated through MATLAB/Simulink simulations. By adjusting the weights assigned to each objective, the impact on the performance of the control system will be demonstrated. The simulated system consists of two two-level, three-phase AFEs that are directly paralleled, sharing a common three-phase AC power supply and a resistive DC load. Each rectifier is equipped with its own set of input inductive filters and corresponding equivalent series resistances. Additionally, both rectifiers are connected to where DC-link capacitor is shared, which is in parallel with the load.

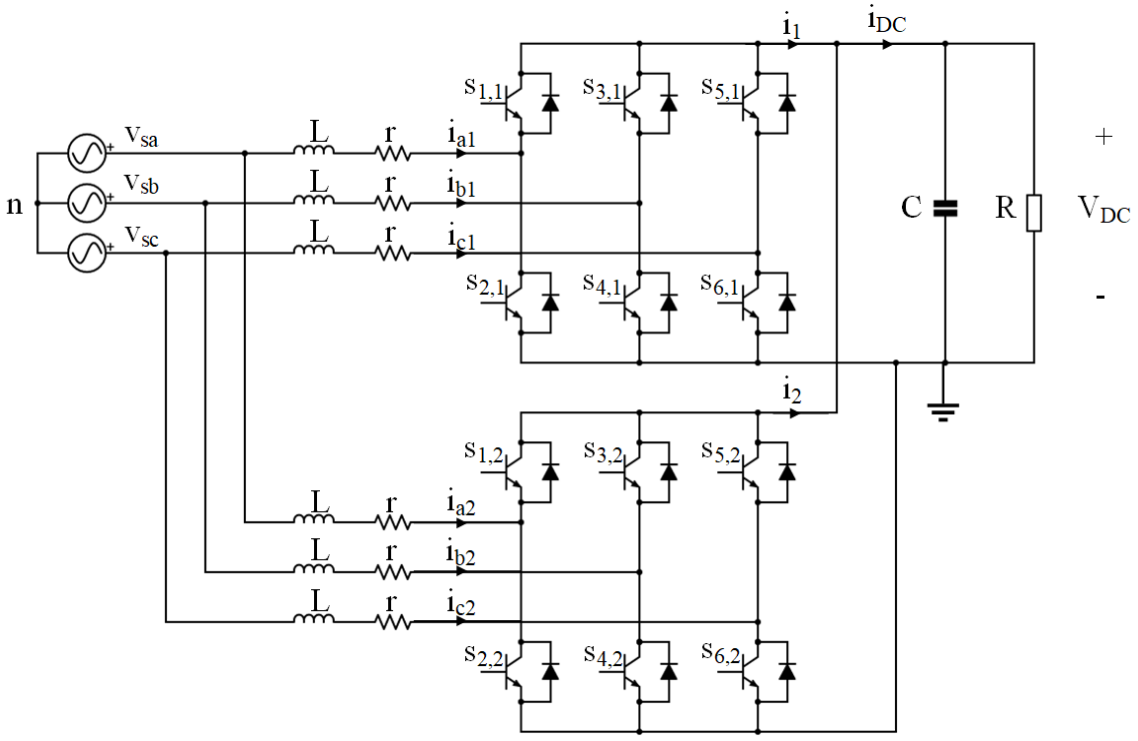

Figure 7.1: The paralleled AFE system under study

7.1 Modeling and Control Derivation

Before discussing the simulation results of the system, it is important to explain how the controlled switching model was derived. For voltage regulation and ZSCC suppression control, the algorithm is based on the work of Tarisciotti et al. [54]. Although the algorithm is detailed in the paper, the most important parts will be addressed in the following section.

Figure 7.1 shows the paralleled rectifiers that are studied in this section. In order to derive a model predictive control, first Kirchhoff's voltage law (KVL) is used to model the AC side of each individual converter. The following KVL equations are obtained:

$$v_{sa}(t) = L\frac{di_{ax}(t)}{dt} + ri_{ax}(t) + s_{ax}(t)V_{DC}(t) \tag{7.1}$$

$$v_{sb}(t) = L\frac{di_{bx}(t)}{dt} + ri_{bx}(t) + s_{bx}(t)V_{DC}(t) \tag{7.2}$$

$$v_{sc}(t) = L\frac{di_{cx}(t)}{dt} + ri_{cx}(t) + s_{cx}(t)V_{DC}(t) \tag{7.3}$$

where $v_{sa}(t)$, $v_{sb}(t)$, and $v_{sc}(t)$, are the line voltages, $i_{ax}(t)$, $i_{bx}(t)$, and $i_{cx}(t)$ are the line currents of the x^{th} converter, $V_{DC}(t)$ is the DC-link voltage, L is the line inductance and r is its equivalent series resistance. The single leg state of the x^{th} converter is represented by $s_{ax}(t)$, $s_{bx}(t)$, and $s_{cx}(t)$, calculated as:

$$s_{ax}(t) = s_{1x}(t) - s_{2x}(t) \tag{7.4}$$

$$s_{bx}(t) = s_{3x}(t) - s_{4x}(t) \tag{7.5}$$

$$s_{cx}(t) = s_{5x}(t) - s_{6x}(t) \tag{7.6}$$

where $s_{1x}(t)$ ... $s_{6x}(t)$ represent the x^{th} converter single switch state, where it is equal to 1 if the switch is ON and 0 if the switch is OFF.

Kirchhoff's Current Law (KCL) is used to model the DC side of each individual converter in the system. By applying KCL, a unified DC model for both the converters connected in parallel can be expressed as:

$$\sum_{x=1} i_x(t) = C\frac{dV_{DC}(t)}{dt} + \frac{V_{DC}(t)}{R} \tag{7.7}$$

where $i_x(t)$ is the current generated by the x^{th} converter. To further refine the model, $i_x(t)$ is expressed as function of the single leg switching state and line currents as follows:

$$i_x(t) = \sum_{i=a,b,c} s_{ix}(t) i_{ix}(t) \tag{7.8}$$

where $s_{ix}(t)$ represents the switching state of the x^{th} converter and $i_{ix}(t)$ represents the line current associated with the x^{th} converter and phase i (a, b, or c).

To predict the current waveforms on the AC side of the converter, equations 7.1,7.2, and 7.3 are discretized using the forward Euler derivative approximation. This approximation converts the differential equations into difference equations as shown by the following:

$$\frac{dx}{dt} = \frac{x(k+1) - x(k)}{T_{sw}} \tag{7.9}$$

where T_{sw} is the switching period. Applying this approximation to equations 7.1, 7.2, and 7.3 results

in the following predictive current equations:

$$i_{ax}(k+1) = \frac{T_{sw}}{L}[V_{sa}(k) - ri_{ax}(k) - s_{ax}(k)V_{DC}(k)] + i_{ax}(k) \tag{7.10}$$

$$i_{bx}(k+1) = \frac{T_{sw}}{L}[V_{sb}(k) - ri_{bx}(k) - s_{bx}(k)V_{DC}(k)] + i_{bx}(k) \tag{7.11}$$

$$i_{cx}(k+1) = \frac{T_{sw}}{L}[V_{sc}(k) - ri_{cx}(k) - s_{cx}(k)V_{DC}(k)] + i_{cx}(k) \tag{7.12}$$

where $i_{ax}(k+1)$, $i_{bx}(k+1)$, and, $i_{cx}(k+1)$ are the predicted currents at the next time step for phases a, b, and c, respectively. They are calculated based on the previous/current line currents ($i_{ax}(k)$, $i_{bx}(k)$, and $i_{cx}(k)$), phase voltages ($V_{sa}(k)$, $V_{sb}(k)$, and $V_{sc}(k)$), switching states ($s_{ax}(k)$, $s_{bx}(k)$, and $s_{cx}(k)$), inductor equivalent series resistance r, and DC voltage $V_{DC}(k)$. The inductance L and the switching period T_{sw} are used in the equation to capture the change in current over time. By iteratively solving these equations, the current waveforms on the AC side of the converters can be accurately predicted.

The forward Euler approximation can also be applied to the DC side term. By applying the approximation to equation 7.7 an approximation of the DC-link voltage is obtained as follows:

$$V_{DC}(k+1) = \frac{T_{sw}}{C}\left[i_1(k) + i_2(k) - \frac{V_{DC}(k)}{R}\right] + V_{DC}(k) \tag{7.13}$$

where $V_{DC}(k+1)$ is the predicted DC voltage. This voltage is calculated based on the previous/current DC bus voltage ($V_{DC}(k)$) and the output currents of each converter ($i_1(k)$ and $i_2(k)$). The capacitance C and the switching period T_{sw} are used in the equation to capture the change in voltage over time.

The predictive DC voltage obtained from this equation is incorporated into a cost function term. This cost function term serves two purposes: to maintain the reference DC voltage across the load and to reduce the transient time required for the load voltage to reach a steady-state. The cost function term associated with these characteristics can be expressed as:

$$G_{DC} = \sqrt{[V_{DC}(k+2) - V^*_{DC}(k)]^2} \tag{7.14}$$

where $V^*_{DC}(k)$ represents the user-defined reference DC voltage.

Moving forward, it is also important to discuss how the MPC algorithm calculates and

manages the zero-sequence circulating current. Building upon the work of Zhihong et al. [61], Tarisciotti et al. [54] comes develop a method to determine the zero-sequence state for each paralleled converter by modifying the previously derived KVL and KCL equations. The zero-sequence state for the x^{th} converter can be represented by the equation:

$$s_{zx}(k) = \sum_{i=a,b,c} s_{ix}(k) \tag{7.15}$$

Similarly, a zero-sequence line current component for the x^{th} converter can be found by the equation:

$$i_{zx}(k) = \sum_{i=a,b,c} i_{ix}(k) \tag{7.16}$$

Using equations 7.15 and 7.16, the zero-sequence power flowing through the x^{th} converter can be calculated as:

$$P_{zx}(k) = \frac{1}{3} s_{zx}(k) V_{DC}(k) i_{zx}(k) \tag{7.17}$$

These zero-sequence power calculations enable the creation of a cost function term to minimize the circulating zero-sequence power. The cost function term used for this purpose is given by the following equation:

$$G_z = \sqrt{\sum_{x=1} P_{zx}^2(k+2)} \tag{7.18}$$

where $P_{zx}^2(k+2)$ represents the zero-sequence power for each converter at the (k+2) time step.

The final component of the algorithm proposed by Tarisciotti et al. [54] focuses on the management of active and reactive power, which is crucial for ensuring the converter operates optimally and with a unity power factor. The first step in active and reactive power management is the calculation of these power quantities. The active power and reactive power managed by the x^{th} converter can be determined by the following equations:

$$P_x(k) = V_{sa}(k) i_{ax}(k) + V_{sb}(k) i_{bx}(k) + V_{sc}(k) i_{cx}(k) \tag{7.19}$$

$$Q_x(k) = \frac{1}{\sqrt{3}} V_{bc}(k) i_{ax}(k) + V_{ca}(k) i_{bx}(k) + V_{ab}(k) i_{cx}(k) \tag{7.20}$$

where $V_{ab}(k)$, $V_{bc}(k)$. and $V_{ca}(k)$ are the line-to-line voltages which can be solved from the line-to-neutral voltages using the equations:

$$V_{ab}(k) = V_{sa}(k) - V_{sb}(k) \tag{7.21}$$

$$V_{bc}(k) = V_{sb}(k) - V_{sc}(k) \tag{7.22}$$

$$V_{ca}(k) = V_{sc}(k) - V_{sa}(k) \tag{7.23}$$

An active power reference for the DC load power P^*_{DC} is used to calculate the amount of power required by the load. This power reference is calculated by the equation:

$$P^*_{DC}(k) = \frac{1}{2} \frac{C}{K T_{sw}} [V^2_{DC}(k) - V^{*2}_{DC}(k)] - \frac{V^2_{DC}(k)}{R} \tag{7.24}$$

Here, K represents the number of sampling intervals necessary to reach the desired voltage reference V^*_{DC}. Additionally, an active power reference P^*_x and reactive power reference Q^*_x for the power circulating through the converters, contributed by the x^{th} converter can be defined by the user. Having power circulating through the converters may be well-suited for testing purposes, so that excessive power from the grid is not used. However, this is not desired for the simulations and so these two references are set to 0. Using this information a total active power reference for the x^{th} converter can be calculated as:

$$P^*_{Total,x}(k) = P^*_x(k) + \frac{P^*_{DC}(k)}{2} \tag{7.25}$$

Using the calculated power quantities and references, a cost function can be created to manage the active and reactive power supplied by the x^{th} converter, expressed as:

$$G_x = \sqrt{[P_x(k+2) - P^*_{Total,x}(k)]^2 + [Q_x(k+2) - Q^*_x(k)]^2} \tag{7.26}$$

where $P_x(k+2)$ and $Q_x(k+2)$ represent the active and reactive powers for the x^{th} converter at time step (k+2), while $P^*_{Total,x}(k)$ and $Q^*_x(k)$ represent their respective power references.

After covering the important equations and cost functions in the algorithm for voltage regulation and ZSCC suppression, it is crucial to describe the overall flow of the algorithm. The MPC algorithm uses the predictive equations 7.10, 7.11, 7.12, and 7.13 to forecast the AC line currents and DC-link voltage for all eight possible switching states of each converter. These predicted values are then used to predict the active, reactive, and zero-sequence powers associated with each converter are calculated using equations 7.19, 7.20, and 7.17, respectively. Lastly, at the end of each sampling instant, the switching states of the two converters are applied to the system that minimize the following cost:

$$G = \sum_{x=1} G_x + w_{DC} G_{DC} + w_z G_z \tag{7.27}$$

where w_{DC} is the weight associated with DC voltage cost function term and w_z is the weight associated with the ZSCC suppression cost function term.

Now that the control derivation for the voltage regulation and ZSCC suppression has been covered, it is important to discuss the modeling and control derivation used for ATM. The modeling aspect employed for ATM was extensively addressed earlier in this thesis, specifically in sections 5.2.1 and 5.2.2, and is based on the work by Gokhan Ozkan [38].

The control strategy for ATM involves calculating the predicted conduction and switching losses associated with the next potential switching states. This is done by inputting the predicted line currents and predicted DC voltages for each possible future switching state into the conduction loss equation (equation 2.1) and the switching loss equation (equation 2.3). By doing so, the total power loss for each IGBT under every potential future switching state can be determined through simple addition. Subsequently, the predicted total power losses for each IGBT in the x^{th} converter are summed as follows:

$$G_{loss,x} = \sum_{l=1} P^l_{loss} \tag{7.28}$$

where l represents each IGBT in a converter and P_{loss} represents the total predicted power loss for each IGBT. This term is then added onto the cost function shown in 7.27 in order to achieve a cost function that not only optimizes the system's voltage regulation and ZSCC suppression, but also

achieves a form of ATM. The new cost function is given as:

$$G = \sum_{x=1} G_x + w_{DC} G_{DC} + w_z G_z + w_{loss} \sum_{x=1} G_{loss,x} \tag{7.29}$$

where w_{loss} is the weight associated with power loss cost function term that is used to achieve ATM.

The predicted power losses for each IGBT are then fed as inputs to third-order Cauer networks that resembling the network depicted in figure 5.2. The voltage measured across the first node each Cauer network corresponds to the predicted junction temperature of each IGBT. After each sampling instant, all predicted temperatures are set as the instantaneous temperature as there are no sensors used to keep track of instantaneous temperature measurements in the simulations.

It is worth noting that in Equation 7.28, the cost function associated with ATM of the converters does not directly influence the temperature but rather affects the power losses of each IGBT in the converters, subsequently influencing the junction temperatures of all devices in the converters. Power losses are modified by the algorithm by varying the switching frequencies of devices in each converter. As the weight for the power loss cost function increases, priority is given to reducing power losses, leading to fewer switching events. Consequently, this reduction in power losses results in a decrease in IGBT junction temperatures.

7.2 Control Algorithm Validation

The paralleled AFEs in the system are modeled using the Simscape Electrical block sets in MATLAB/Simulink, as shown by figure 7.2. The control algorithm is implemented for the simulation using a MATLAB S-function within MATLAB/Simulink, as illustrated by figure 7.3. The measurements taken in from the control system are used as inputs to the MATLAB S-function block. This block subsequently returns converter switching states, which are fed back to the control system. Additionally, the MATLAB S-function provides predicted junction temperature values for each IGBT. The specific system parameters used in the simulations are outlined in table 7.4.

Three unnormalized weights are employed to control the three objectives in the system. Although these weights exhibit diminishing returns on the control of the objectives, as demonstrated in this section, they do not possess any specific bounds on their minimum and maximum values. Consequently, there exists an infinite range of weight combinations that can be chosen. However, for the purpose of this section, only a limited number of combinations are showcased to illustrate the

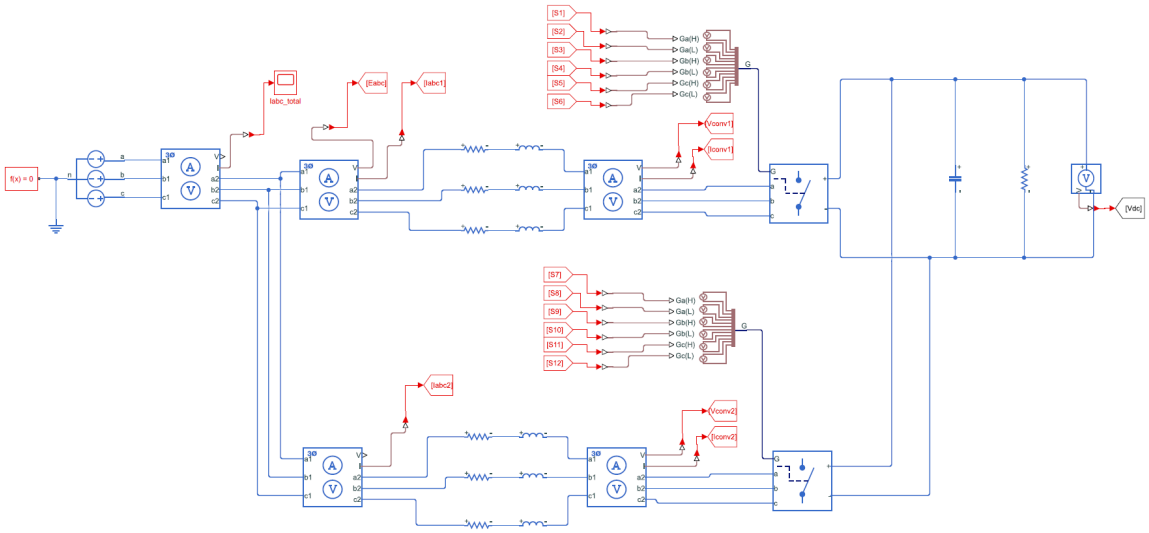

Figure 7.2: Control system constructed using Simscape Electrical blocks

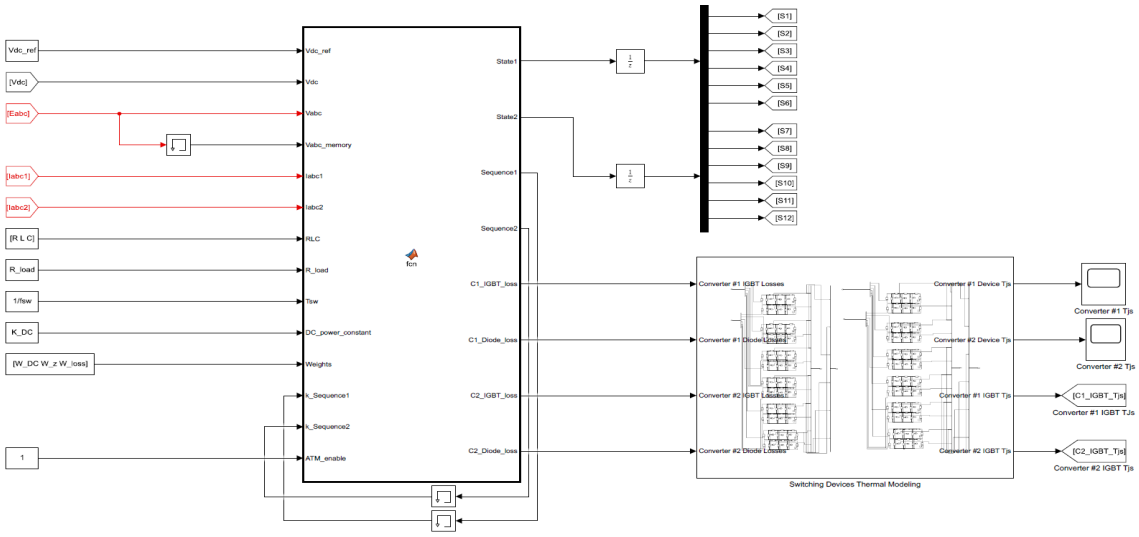

Figure 7.3: MATLAB S-function containing the control algorithm

Variables and Parameters	Symbol	Value
AC-side Line-to-Line RMS Voltage	e	230 V
Frequency	f	50 Hz
DC-link Reference Voltage	V_{DC}*	650 V
DC-link Initial Voltage	V_{DC}	600 V
Control Sampling Time	T_{sw}	50 µs
Load Resistance	R	100 Ω
DC-link Capacitance	C	6 mF
AC-side Inductance	L	10 mH
AC-side Equivalent Series Resistance	r	0.1 Ω
Converter Ambient Temperature	T	30°C
DC Power Constant	K	80

Table 7.4: System variables and parameters used for the MATLAB/Simulink simulations

effectiveness of the control algorithm. Throughout this section, as the three cost function weights are altered, the corresponding instantaneous converter input currents, linked to the instantaneous line voltages, are presented. Furthermore, this section features three monitors that track the status of the key objectives: the DC bus voltage, the zero-sequence current for each converter, and the temperature of all six IGBTs in each converter. By observing the behavior of these variables, the impact of varying the cost function weights on the control system's performance can be thoroughly examined.

For initial validation of the voltage regulation and ZSCC suppression components in the algorithm, it is logical to proceed in a similar manner as Tarisciotti et al. [54] and make sure that comparable system performance is achieved. Therefore, the first set of system measurements presented in figures 7.5 and 7.6 are simulations where w_{DC} is set to 2000, w_z is set to 0.1, and w_{loss} is set to 0. These measurements show that the DC voltage rapidly reaches a steady state within approximately 0.02 seconds, while the ZSCC is effectively suppressed, as indicated by its reduction to zero. Figure 7.7 provides a closer view of the load DC voltage, revealing an actual value of 650.6 V, which translates to a very acceptable error margin of about 0.09

Subsequently, a different set of system measurements, depicted in Figures 7.8 and 7.9, is obtained by running the simulation with w_z set to 0, effectively disabling ZSCC suppression. Consequently, zero-sequence currents with equal magnitude but opposite polarity now flow through

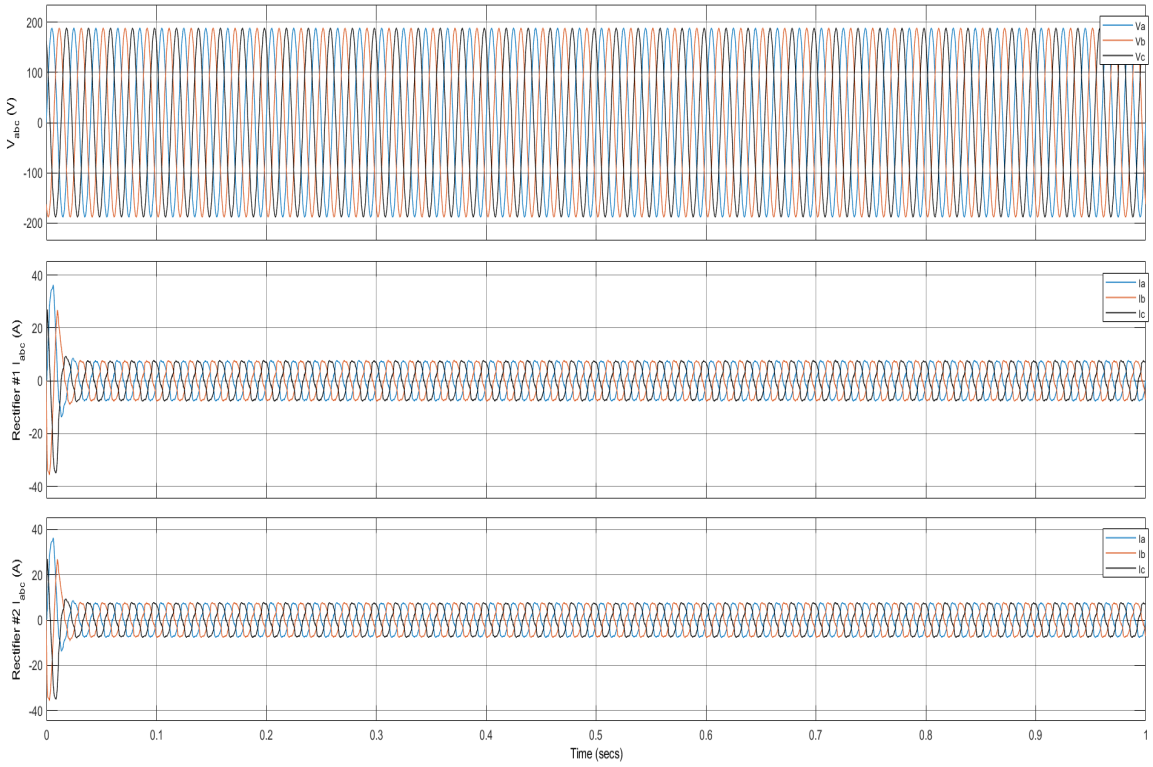

Figure 7.5: System measurements for $w_{DC} = 2000$, $w_z = 0.1$, and $w_{loss} = 0$

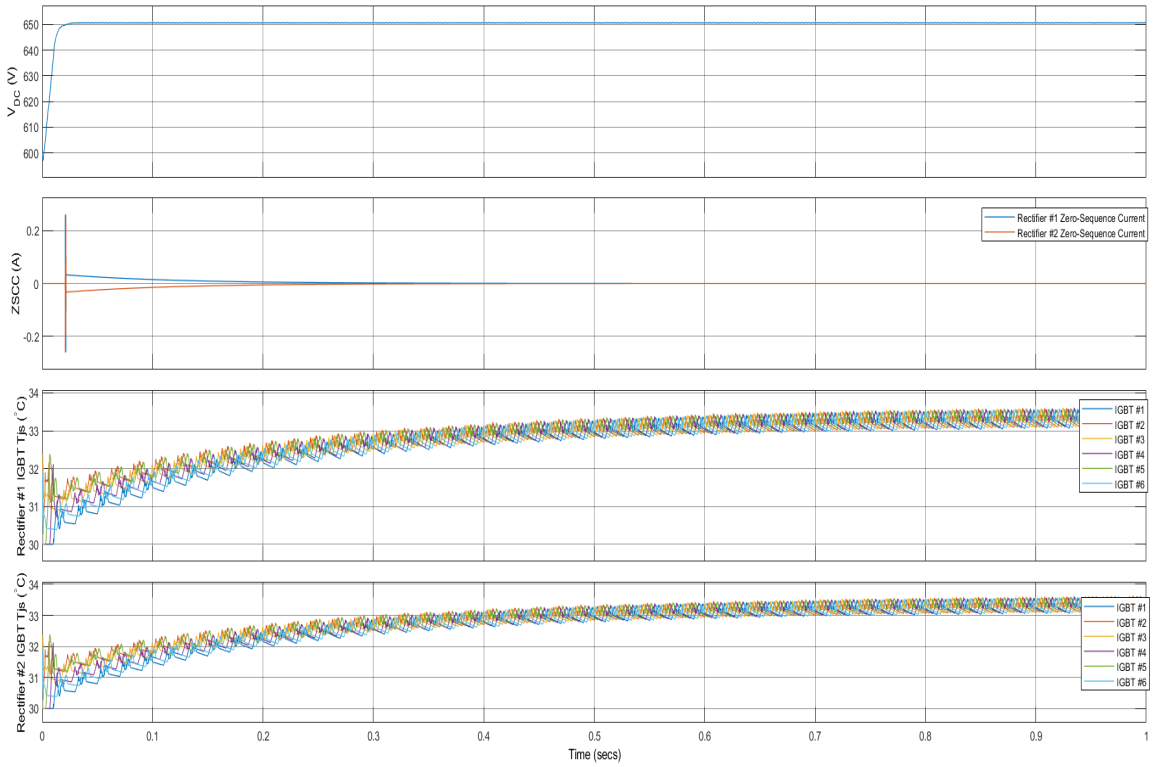

Figure 7.6: Objective measurements for $w_{DC} = 2000$, $w_z = 0.1$, and $w_{loss} = 0$

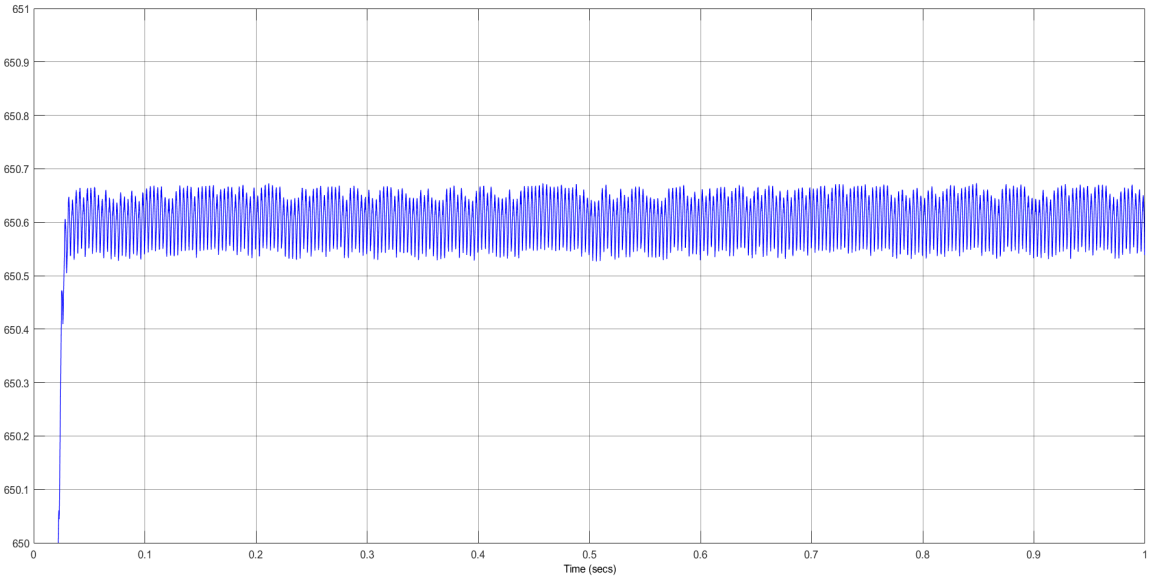

Figure 7.7: Zoomed in view of DC voltage for $w_{DC} = 2000$, $w_z = 0.1$, and $w_{loss} = 0$

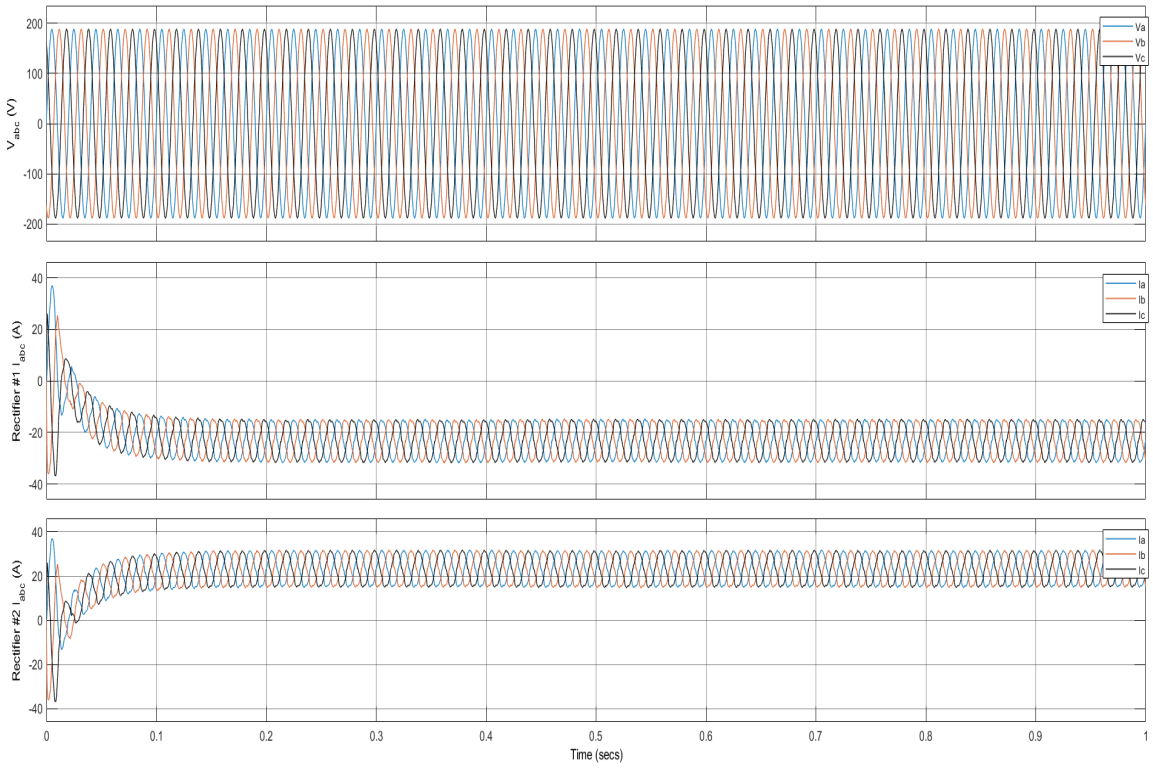

Figure 7.8: System measurements for $w_{DC} = 2000$, $w_z = 0$, and $w_{loss} = 0$

the converters. Figure 7.10 shows a zoomed in view the load DC voltage, revealing an actual value of 650.1 V, indicating an error margin of approximately 0.015%. As ZSCC suppression is no longer prioritized, the algorithm devotes greater effort to achieving the reference voltage, resulting in a more precise value with even shorter transient time.

It is crucial to note that the presence of ZSCC introduces a current offset in both converters, leading to the utilization of only the bottom IGBTs (IGBT #2, IGBT #4, and IGBT #6) in the top converter, while only the top IGBTs (IGBT #1, IGBT #3, and IGBT #5) of the bottom converter are utilized. Consequently, the utilized IGBTs experience significant heating, thereby reducing their lifespan, while the unused IGBTs remain at a much cooler, near ambient temperature. This further show the significance of eliminating ZSCC in the converters when utilizing synchronized control. And it is worth highlighting that the two sets of weighting factors employed in the simulations mirror the system performance outcomes presented in Tarisciotti et al. [54], thus validating the control algorithm's capabilities in voltage regulation and ZSCC suppression.

The thermal capabilities of the control algorithm become apparent when revisiting the

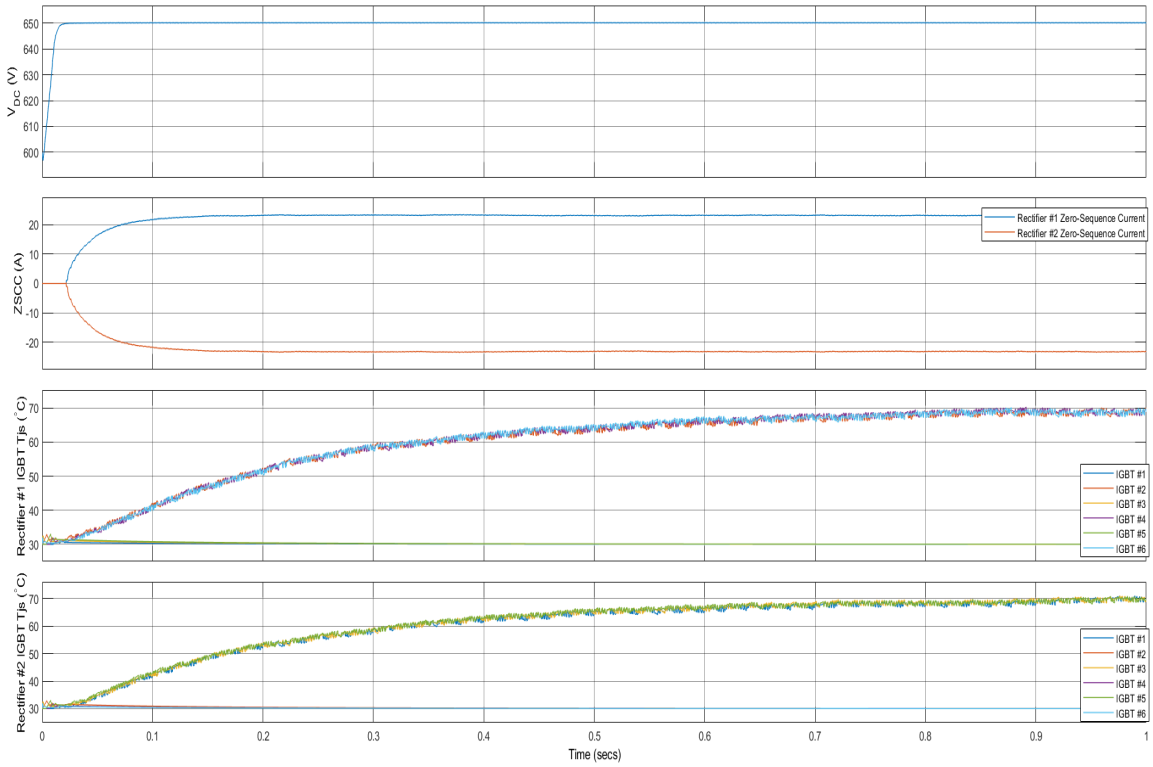

Figure 7.9: Objective measurements for $w_{DC} = 2000$, $w_z = 0$, and $w_{loss} = 0$

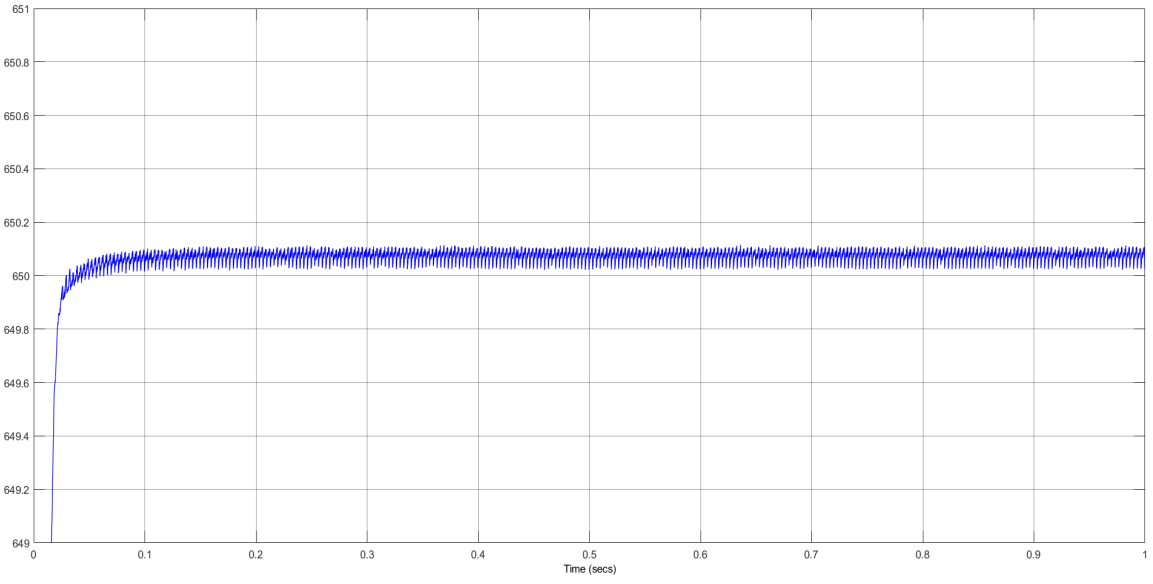

Figure 7.10: Zoomed in view of DC voltage for $w_{DC} = 2000$, $w_z = 0$, and $w_{loss} = 0$

previous examples and increasing the weight assigned to power loss. For instance, considering the scenario where $w_{DC} = 2000$ and $w_z = 0.1$, but now adding a power loss weight of $w_{loss} = 10$, the resulting system measurements are shown in figures 7.11 and 7.12. A comparison with the simulation results where $w_{loss} = 0$, as depicted in figure 7.6, reveals that increasing w_{loss} to 10 extends the time required for the load voltage to reach a steady state from approximately 0.02 seconds to about 0.05 seconds. This slight delay is due to a decrease in the priority given to the reference voltage, as power loss priority is introduced. Consequently, the transient time to reach steady state is sacrificed to reduce the initial thermal transient temperatures. When $w_{loss} = 0$, there is a sharp increase in temperature at the start of the simulation as the voltage transients to steady state, which is not observed when $w_{loss} = 10$. Instead, a more gradual temperature increase is observed during the early simulation period. It is worth noting that the jump in temperature during the transient is relatively small due to the high thermal dissipation abilities of the chosen IGBT module and heatsink in the simulation. However, for converters with inferior thermal characteristics, the temperature jump could be significantly larger. Additionally, if the load profile is subject to frequent variations, the accumulation of temperature jumps during load transients can negatively impact converter performance. And it can be seen in both scenarios that the temperature of all IGBTs fluctuate around one another meaning that thermal balance is achieved and therefore all IGBTs are stressed evenly.

To gain further insight into the steady-state thermal characteristics of the converter, the value of $w_z$is increased to 100. The system measurements for this scenario, where $w_{DC} = 2000$, w_z= 0.1, and $w_{loss} = 100$, are shown in figures 7.13 and 7.14. Here, it becomes evident that the thermal transients observed during the early stages of the simulation are further reduced, and the steady-state thermal state of both converters decreases from approximately 33.5°C when $w_{loss} = 0$ and $w_{loss} = 10$ to approximately 31.4°C when $w_{loss} = 100$. However, it is important to note that this thermal improvement comes at a significant cost to the DC voltage across the load, as it drops to approximately 450 V and fails to reach anywhere near the reference voltage of 650 V. In addition, it can be seen that all the IGBTs are stressed evenly once again as all IGBT temperatures fluctuate in a similar manner.

Interestingly, even when $w_z$is set to 0, enabling zero-sequence current, the results remain nearly identical when w_{DC}, w_z= 0, and $w_{loss} = 100$, as shown in figures 7.15 and 7.16. This suggests that the thermal weight of 100 takes precedence over the other two objectives, and the

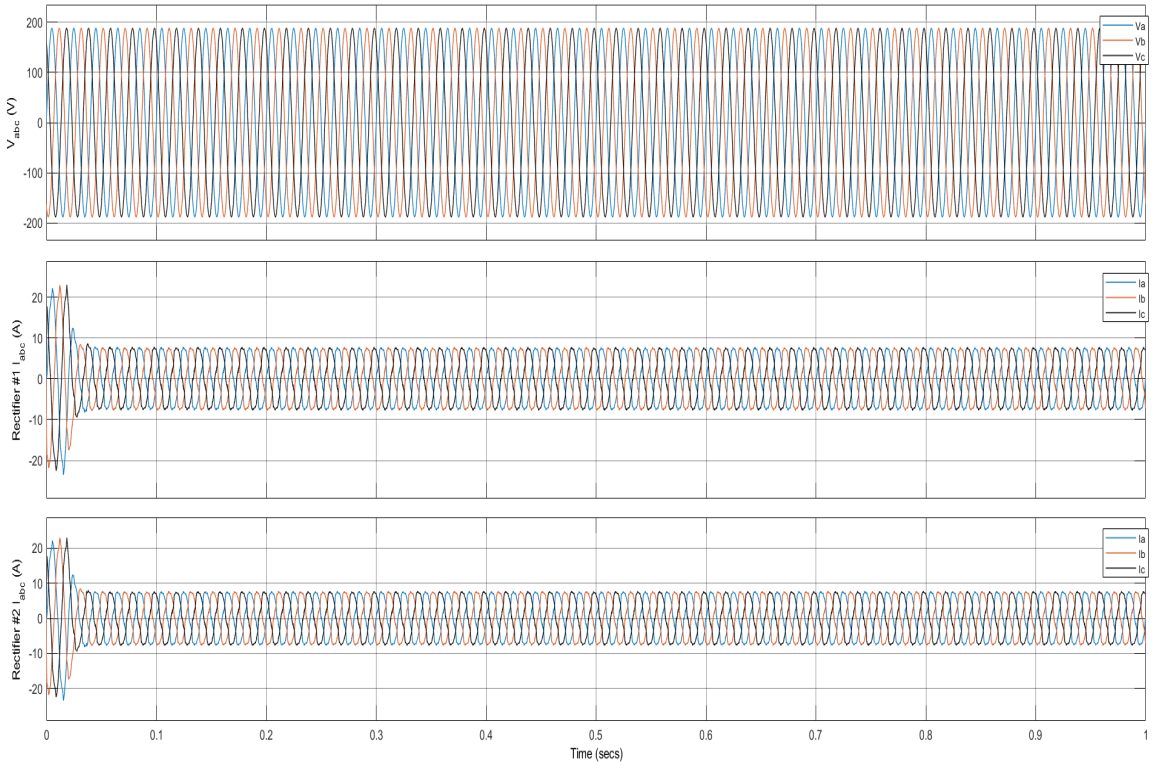

Figure 7.11: System measurements for $w_{DC} = 2000$, $w_z = 0.1$, and $w_{loss} = 10$

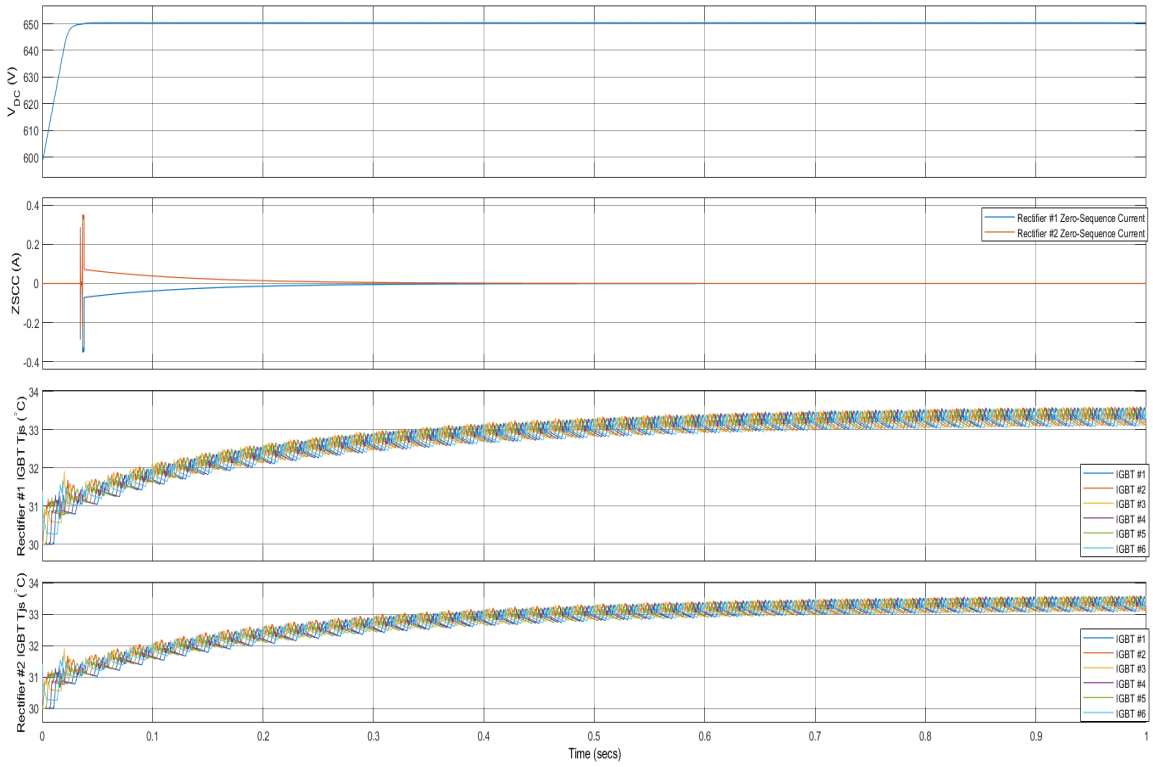

Figure 7.12: Objective measurements for $w_{DC} = 2000$, $w_z = 0.1$, and $w_{loss} = 10$

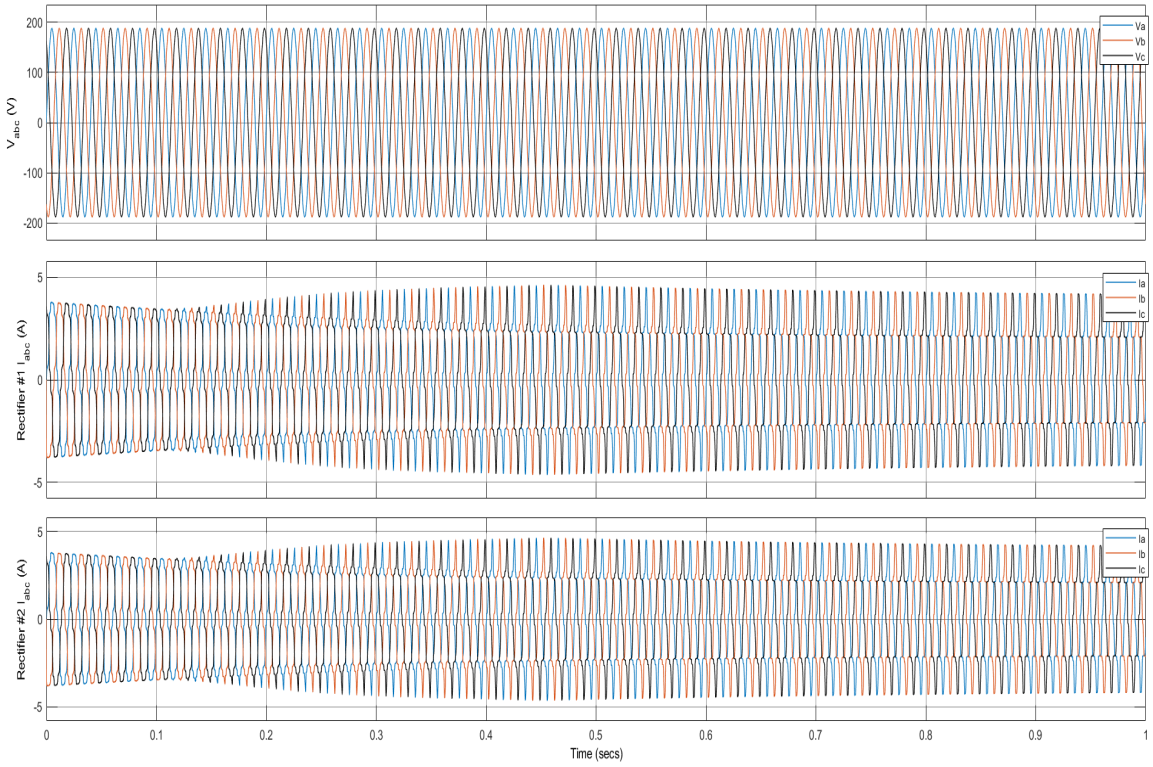

Figure 7.13: System measurements for $w_{DC} = 2000$, $w_z = 0.1$, and $w_{loss} = 100$

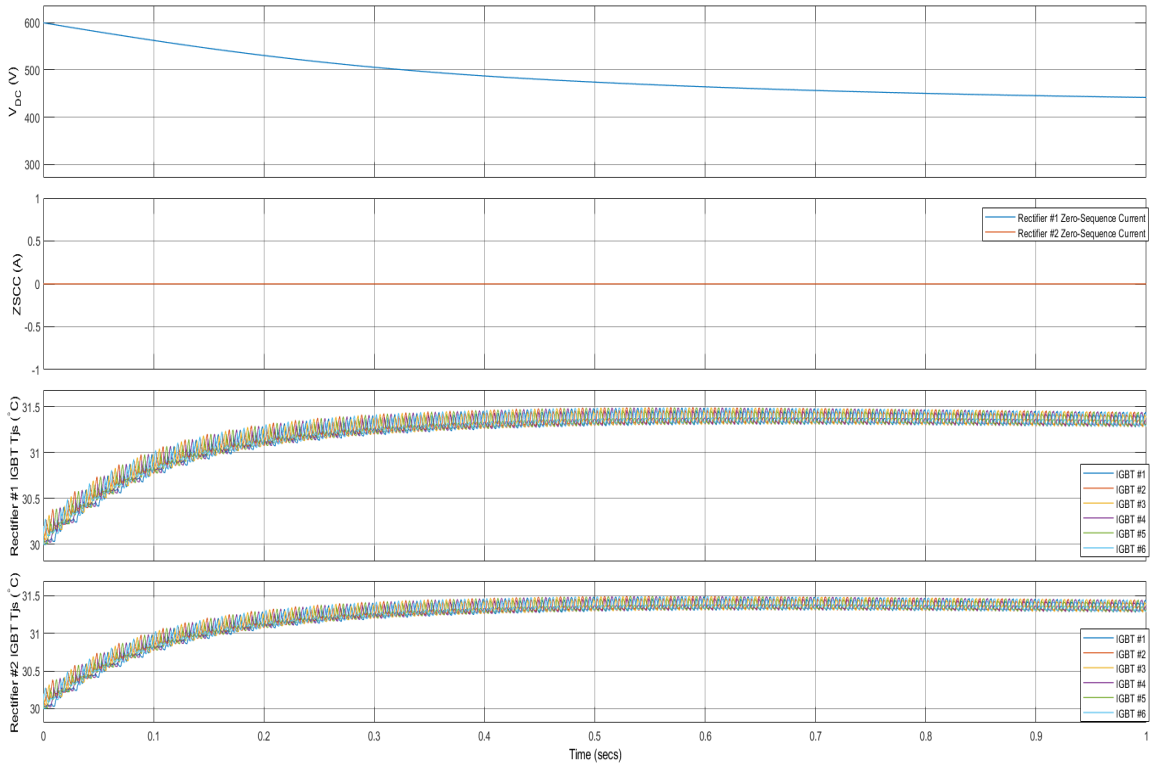

Figure 7.14: Objective measurements for $w_{DC} = 2000$, $w_z = 0.1$, and $w_{loss} = 100$

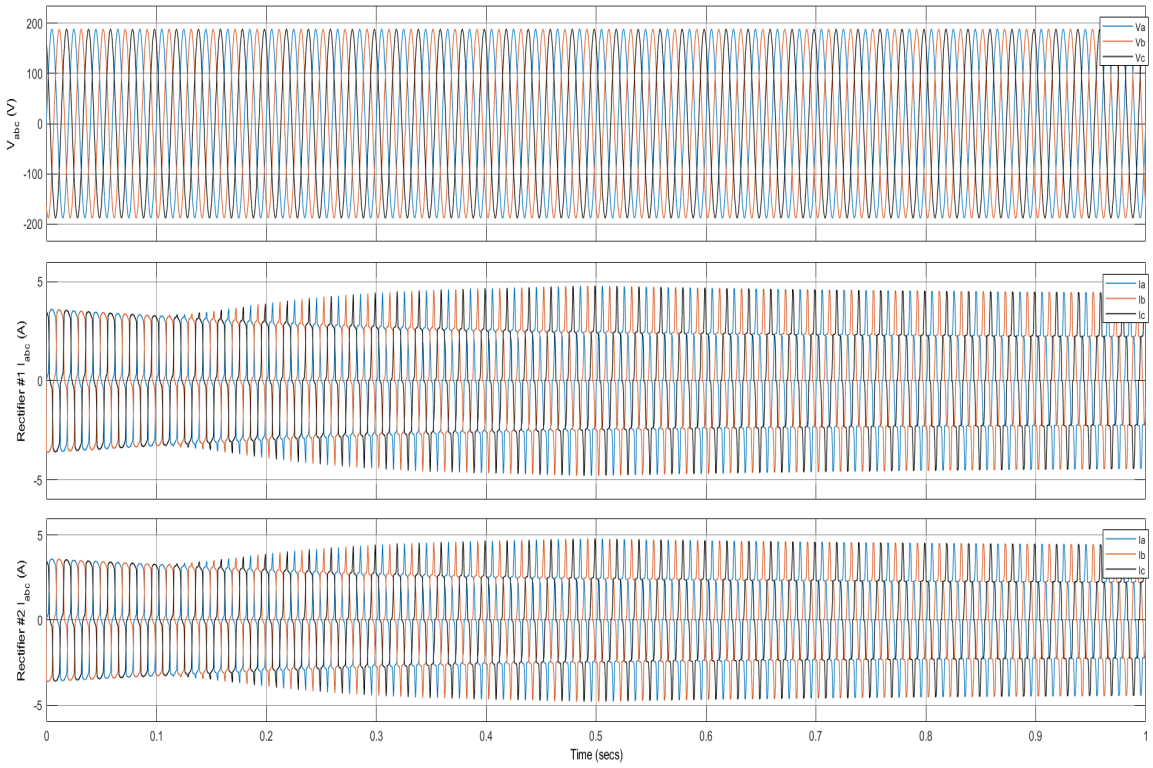

Figure 7.15: System measurements for $w_{DC} = 2000$, $w_z = 0$, and $w_{loss} = 100$

algorithm primarily aims to achieve lower thermal characteristics for the switches in the converters. Coincidentally, the solution for achieving the lowest thermal state also results in the elimination of ZSCC. This further highlights the inherent creativity and strength of the MPC approach.

The tuning of weighting factors in the MPC algorithm cannot rely on a standard procedure due to the strong influence of the system's mission profile. The effectiveness of the controller heavily depends on the system's operating conditions and load characteristics, necessitating a customized approach to determine optimal weighting factors tailored to the specific mission profile. Consequently, a mathematical approach for determining the best choice of weights that achieves optimal results for all three key objectives is not available. Instead, various combinations of weights were explored to observe their impact on the three key objectives. However, many combination of weights, seemed to provide satisfactory objective performance, such as the previously examined case where $w_{DC} = 2000$, $w_z = 0.1$, and $w_{loss} = 10$. However, it should be noted that since these weights are unnormalized, there might exist other scaled combinations that yield the same results.

Another significant scenario to consider is when all weights are set to 0. The results are

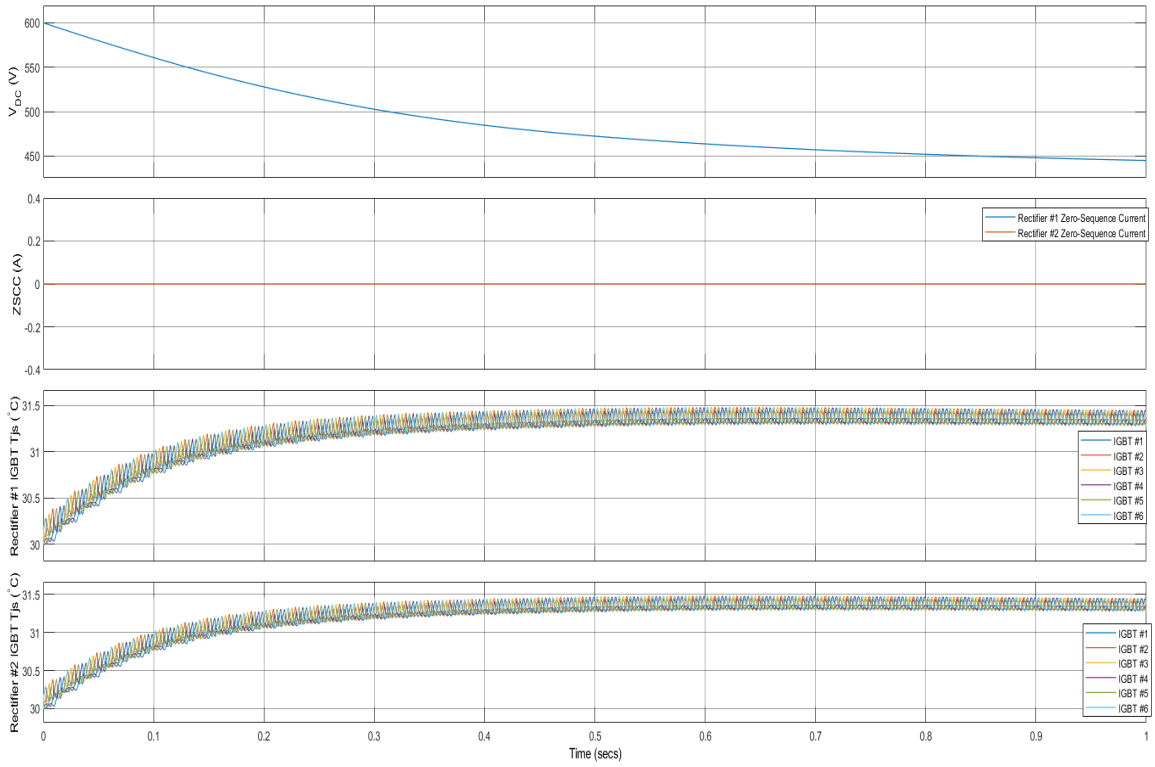

Figure 7.16: Objective measurements for $w_{DC} = 2000$, $w_z = 0$, and $w_{loss} = 100$

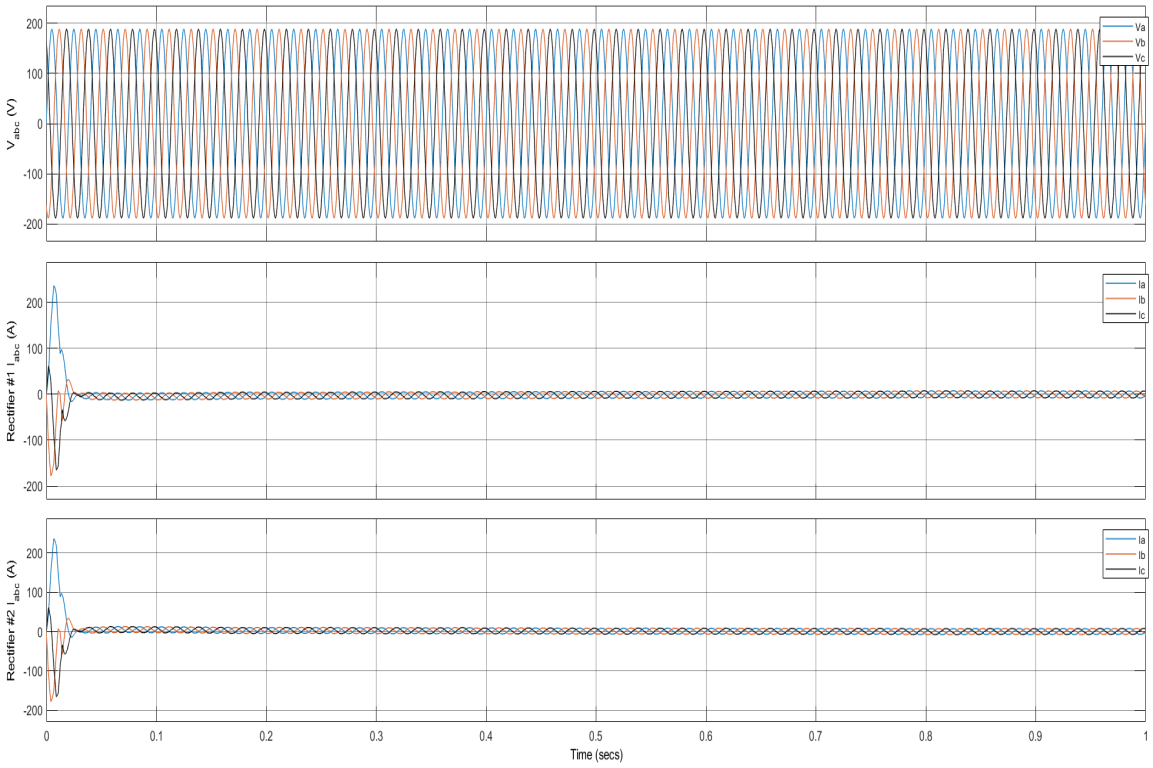

Figure 7.17: System measurements for $w_{DC} = 0$, $w_z = 0$, and $w_{loss} = 0$

depicted in figures 7.17 and 7.18. It is evident that the reference voltage can still be achieved even with $w_{DC} = 0$ due to the G_x cost function terms. These terms not only ensure the reference active and reactive power flow through the converter but also contribute to reaching the reference voltage. However, having w_{DC} set to 0 leads to larger DC voltage undershoot and overshoot during the transient period, as the DC voltage takes more time to reach steady state. Additionally, with $w_{DC} = 0$, there is an increase in zero-sequence current flowing through the converters compared to the case when w_{DC}= 0 and $w_z = 0.1$, as zero-sequence current mitigation is no longer prioritized. Furthermore, with thermal control no longer a priority, the IGBT temperatures in each converter exhibit higher amplitudes and imbalance, resulting in reduced lifetime and reliability of the devices during prolonged operation.

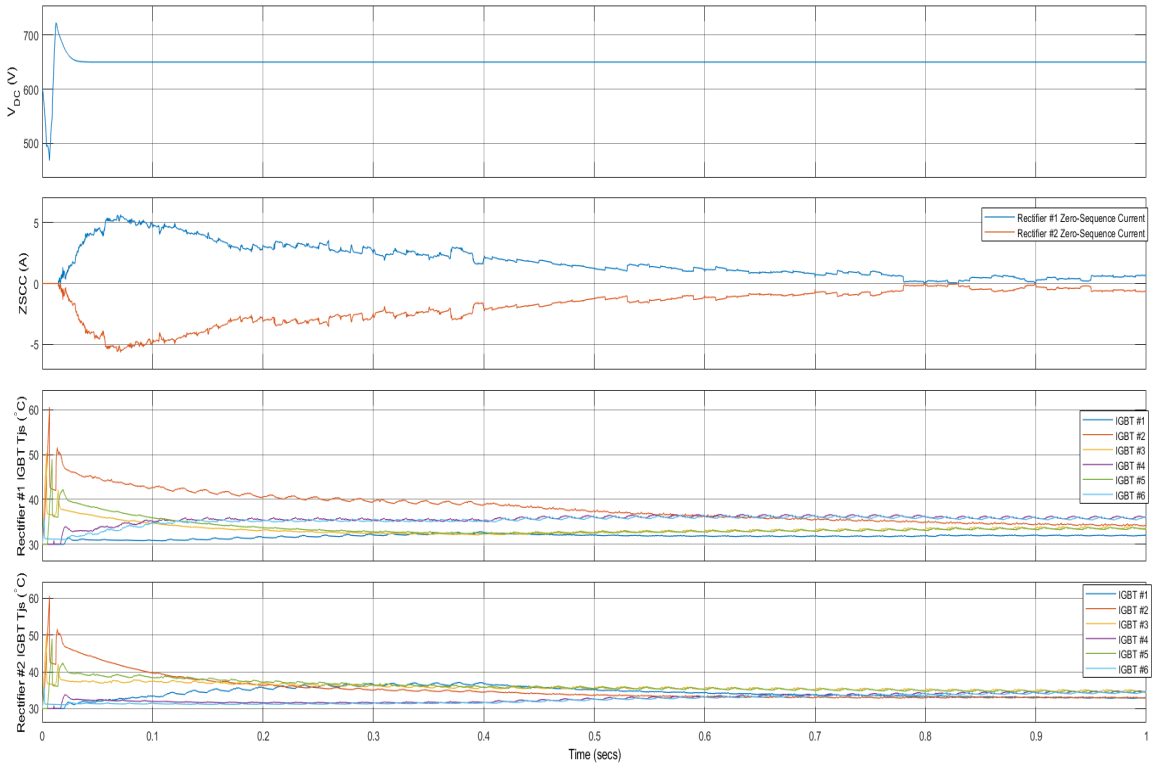

Figure 7.18: Objective measurements for $w_{DC} = 0$, $w_z = 0$, and $w_{loss} = 0$

Chapter 8

Conclusions and Future Work

In conclusion, the results of this study demonstrate the effectiveness of the proposed control algorithm in achieving the key objectives of voltage regulation, zero-sequence current suppression, and thermal management in paralleled power converters. The simulations and analysis conducted show the impact of the MPC algorithm's effectiveness on system performance. Through exploration of various combinations of weights, it was observed that certain combinations could lead to improvements in any of the three key objectives. This validation reinforces confidence in the control algorithm's ability to meet the objectives of power converter control.

The successful validation of the control algorithm presents opportunities for its practical implementation in real-world applications. The demonstrated enhancements in system performance highlight the potential impact of this MPC algorithm in improving the efficiency, stability, and reliability of power conversion systems. Notably, the absence of intrusive temperature sensors allows for further miniaturization and increased power density of power systems. Given the author's awareness of no existing work where all three objectives are met, these findings contribute significantly to the advancement of power converter control techniques, providing a foundation for its practical implementation across diverse power conversion applications, including the Navy's power systems utilizing power electronic building blocks.

8.1 Recommendations for Further Research

Although the employed modeling approach in this work yields sufficient accuracy, future research can explore the use of more complex converter models to better account for system objectives. For instance, the integration of higher-order Cauer networks can provide a more accurate representation of heat propagation within the converter, leading to improved management of system objectives. In addition, the constants used for power loss calculations can be obtained from curve fitting techniques rather than being approximated to achieve more accurate system monitoring.

Additionally, there is potential to conduct hardware-in-the-loop experiments to validate the proposed algorithm using real hardware. This would facilitate testing of the control algorithm's effectiveness in achieving system objective control under various loading scenarios. Furthermore, investigating tuning techniques to identify the optimal combination of weights for achieving overall system performance can further enhance the algorithm's practical applicability.

By addressing these areas of further research, researchers can refine the control algorithm, enhance its accuracy and applicability, and unlock its full potential for real-world power conversion systems.

Bibliography

[1] Pulse-width modulation. [Online; accessed 4-May-2023].

[2] Wide Band Gap Semiconductor Market - Global Industry Analysis, Size, Share, Growth, Trends and Forecast 2017 - 2025. `https://www.transparencymarketresearch.com/wide-band-gap-semiconductor-market.html`.

[3] M. Andresen and M. Liserre. Impact of active thermal management on power electronics design. *Microelectronics Reliability*, 54(9):1935–1939, 2014. SI: ESREF 2014.

[4] B. Jayant Baliga. Igbt applications: Defense. In *The IGBT Device: Physics, Design and Applications of the Insulated Gate Bipolar Transistor*, chapter 14, pages 451–488. Binghamton: Elsevier Science Technology Books, 2015.

[5] Jens Birk and Bjorn Andresen. Parallel-connected converters for optimizing efficiency, reliability and grid harmonics in a wind turbine. In *2007 European Conference on Power Electronics and Applications*, pages 1–7, 2007.

[6] Patricio Cortes, Jose Rodriguez, Patrycjusz Antoniewicz, and Marian Kazmierkowski. Direct power control of an afe using predictive control. *IEEE Transactions on Power Electronics*, 23(5):2516–2523, 2008.

[7] Neta C Crawford. Pentagon Fuel Use, Climate Change, and the Costs of War. Technical report, Watson Institute, Brown University, November 2019.

[8] Juan W Dixon. *Three-phase controlled rectifiers*. Butterworth-Heinemann, 2011.

[9] J.W. Dixon and B.T. Ooi. Series and parallel operation of hysteresis current-controlled pwm rectifiers. *IEEE Transactions on Industry Applications*, 25(4):644–651, 1989.

[10] ECESTUFF4U.com. IGBT Construction. [Online; accessed 11-October-2022].

[11] Electronics Tutorials. Insulated Gate Bipolar Transistor. [Online; accessed 10-October-2022].

[12] Robert W. Erickson and Dragan Maksimović. *Fundamentals of Power Electronics*. Springer, 3 edition, 2020.

[13] Terry Ericsen. "The Second Electronic Revolution" (It's All About Control). In *2009 Record of Conference Papers - Industry Applications Society 56th Annual Petroleum and Chemical Industry Conference*, pages 1–10, 2009.

[14] Terry Ericsen, Yuri Khersonsky, Perry Schugart, and Peter Steimer. PEBB - Power Electronics Building Blocks, from Concept to Reality. In *2006 3rd IET International Conference on Power Electronics, Machines and Drives - PEMD 2006*, pages 12–16, 2006.

[15] P M Fabis, D Shum, and H Windischmann. Thermal modeling of diamond-based power electronics packaging. In *Fifteenth Annual IEEE Semiconductor Thermal Measurement and Management Symp.(Cat. No.99CH36306)*, pages 98–104. IEEE, 1999.

[16] Johannes Falck, Markus Andresen, and Marco Liserre. Active thermal control of igbt power electronic converters. In *IECON 2015 - 41st Annual Conference of the IEEE Industrial Electronics Society*, pages 000001–000006, 2015.

[17] Amin Ghazanfari, Christian Perreault, and Karim Zaghib. Ev/hev industry trends of wide-bandgap power semiconductor devices for power electronics converters. In *2019 IEEE 28th International Symposium on Industrial Electronics (ISIE)*, pages 1917–1923, 2019.

[18] A.E. Ginart, I Ali, Jose Celaya, Patrick Kalgren, Poll S, and M Roemer. Modeling sio2 ion impurities aging in insulated gate power devices under temperature and voltage stress. 01 2010.

[19] Yasin Gunaydin, Saeed Jahdi, Olayiwola Alatise, Jose Ortiz Gonzalez, Ruizhu Wu, Bernard Stark, Mohammad Hedayati, Xibo Yuan, and Phil Mellor. Performance of wide-bandgap gallium nitride vs silicon carbide cascode transistors. In *2020 IEEE Energy Conversion Congress and Exposition (ECCE)*, pages 239–245, 2020.

[20] Zhao Han, Xiaoli Wang, Baochen Jiang, and Jingru Chen. A control strategy for suppressing zero-sequence circulating current in paralleled three-phase voltage-source pwm converters. *Applied Sciences*, 10(5), 2020.

[21] Boyang Hu, Swamidoss Sathiakumar, and Yash Shrivastava. 180-degree commutation system of permanent magnet brushless dc motor drive based on speed and current control. In *2009 Second International Conference on Intelligent Computation Technology and Automation*, volume 1, pages 723–726, 2009.

[22] Xianjin Huang, Feng Mu, Yixin Liu, Yuhan Wu, and Hu Sun. Asynchronous gate signal driving method for reducing current imbalance of paralleled igbt modules caused by driving circuit parameter difference. *IEEE Access*, 9:86523–86534, 2021.

[23] Petros Karamanakos and Tobias Geyer. Guidelines for the Design of Finite Control Set Model Predictive Controllers. *IEEE Transactions on Power Electronics*, 35(7):7434–7450, 2020.

[24] Masoud Karimi-Ghartemani. *Modeling and Control of Modern Electrical Energy Systems*. IEEE Press, 2022.

[25] T. Kawabata and S. Higashino. Parallel operation of voltage source inverters. *IEEE Transactions on Industry Applications*, 24(2):281–287, 1988.

[26] Sang-Hoon Kim. Chapter 7 - pulse width modulation inverters. In Sang-Hoon Kim, editor, *Electric Motor Control*, pages 265–340. Elsevier, 2017.

[27] James L Kirtley. *Electric Power Principles*. Wiley, 2 edition, 2020.

[28] Gan Lian. The pros and cons of gan family of materials compared with other alternatives regarding optoelectronic applications. In *2020 7th International Forum on Electrical Engineering and Automation (IFEEA)*, pages 149–152, 2020.

[29] Nan Lin, Yuheng Wu, Mohammad Mahmud, Yue Zhao, and Alan Mantooth. Current balancing methods for a high power silicon carbide inverter with paralleled modules. In *2022 IEEE Applied Power Electronics Conference and Exposition (APEC)*, pages 1586–1591, 2022.

[30] Fang Lin Luo, Hong Ye, and Muhammad H. Rashid. *Digital Power Electronics and Applications*. Elsevier Science & Technology, 2005.

[31] Stefanos N. Manias. *Power Electronics and Motor Drive Systems*. Academic Press, 2017.

[32] C.C. Marouchos. Institution of Engineering and Technology (The IET), 2006.

[33] K. Matsui, Y. Murai, M. Watanabe, M. Kaneko, and F. Ueda. A pulsewidth-modulated inverter with parallel connected transistors using current-sharing reactors. *IEEE Transactions on Power Electronics*, 8(2):186–191, 1993.

[34] Maxim Integrated. Source Resistance: The Efficiency Killer in DC-DC Converter Circuits. Technical report, April 2004.

[35] Flex Power Modules. Using analog isolated power modules in parallel configurations. *Flex Power Modules*, 2021.

[36] M.A. Noroozi, J.S. Moghani, J. Mili Monfared, and H. Givi. Sensorless starting method for brushless dc motors using 180 degree commutation. In *2012 3rd Power Electronics and Drive Systems Technology (PEDSTC)*, pages 57–61, 2012.

[37] Royal Society of Chemistry. Silicon. `https://www.rsc.org/periodic-table/element/14/silicon#:~:text=Silicon%20makes%20up%2027.7%25%20of,(oxygen%20is%20the%20first)`.

[38] G Ozkan. *Active Thermal Management And Fault-Tolerant Control For Switching Power Converters With Sequence-Based Control*. PhD thesis, Florida State University, 2019.

[39] Gokhan Ozkan, Phuong H. Hoang, Payam Ramezani Badr, Chris S. Edrington, and Behnaz Papari. Real-time thermal management for two-level active rectifier with finite control set model predictive control. *International Journal of Electrical Power Energy Systems*, 131:107057, 2021.

[40] Jaeyoung Park, Sungho Jung, and Jung-Ik Ha. Phase current reconstruction with single dc-link current sensor for six-step operation in three phase inverter. In *2015 IEEE Energy Conversion Congress and Exposition (ECCE)*, pages 906–912, 2015.

[41] Mukund R. Patel. *Introduction to Electrical Power and Power Electronics*. CRC Press, 2012.

[42] Zhongyi Quan and Yun Wei Li. Suppressing zero-sequence circulating current of modular interleaved three-phase converters using carrier phase shift pwm. *IEEE Transactions on Industry Applications*, 53(4):3782–3792, 2017.

[43] Muhammad H Rashid. *Power Electronics Handbook*. Elsevier Science & Technology, 2017.

[44] Mohammad Hasan Ravanji, Nima Amouzegar Ashtiani, Mostafa Parniani, and Hossein Mokhtari. Modeling and control of zero-sequence circulating current in parallel converters with space vector modulation. *IEEE Journal of Emerging and Selected Topics in Power Electronics*, 5(1):363–377, 2017.

[45] Marco Rivera, Diego Rojas, and Patrick Wheeler. The selection of cost functions in model predictive control applications. In *2021 21st International Symposium on Power Electronics (Ee)*, pages 1–6, 2021.

[46] Jose Rodriguez and Patricio Cortes. Control of an active front-end rectifier. In *Predictive Control of Power Converters and Electrical Drives*, volume 44, pages 81–98. Wiley, 1st edition, 2012.

[47] J.A. Rossiter. *A First Course in Predictive Control*. CRC Press, 2018.

[48] Alfeu Sguarezi. *Model Predictive Control for Doubly-Fed Induction Generators and Three-Phase Power Converters*. Elsevier, 2022.

[49] Muamer M. Shebani, Tarirq Iqbal, and John E. Quaicoe. An implementation of cable resistance in modified droop control method for parallel-connected dc-dc boost converters. In *2018 IEEE Electrical Power and Energy Conference (EPEC)*, pages 1–6, 2018.

[50] K. Shenai. Potential impact of emerging semiconductor technologies on advanced power electronic systems. *IEEE Electron Device Letters*, 11(11):520–2, November 1990.

[51] K. Shenai, R.S. Scott, and B.J. Baliga. Optimum semiconductors for high-power electronics. *IEEE Transactions on Electron Devices*, 36(9):1811–1823, 1989.

[52] P.K. Steimer. Power electronics building blocks - a platform-based approach to power electronics. In *2003 IEEE Power Engineering Society General Meeting (IEEE Cat. No.03CH37491)*, volume 3, pages 1360–1365, 2003.

[53] S.M. Sze. *Physics of Semiconductor Device*. Wiley Interscience Publication, 1981.

[54] Luca Tarisciotti, Claudio Burgos, Cristian Garcia, and Jose Rodriguez. Finite control set model predictive control of parallel three-phase active rectifiers. In *2020 IEEE International Conference on Industrial Technology (ICIT)*, pages 1071–1076, 2020.

[55] Andrzej M. Trzynadlowski. *Introduction to Modern Power Electronics*. John Wiley & Sons, Incorporated, 2015.

[56] Nicolai U and Wintrich A. *Determining switching losses of SEMIKRON IGBT modules*. SEMIKRON, August 2014. Application Note, AN 1403.

[57] Mario Vražić, Damir Vuljaj, Zlatko Hanić, and Marinko Kovačić. Approach to Ship Power Network Optimization Regarding Total Harmonic Distortion. In *2016 International Conference on Development and Application Systems (DAS)*, pages 207–211, 2016.

[58] Fei (Fred) Wang, Zheyu Jones Zhang, and Edward A. Characterization of wide bandgap power semiconductor devices, January 2018.

[59] Jinping Wang, Fanyu Hu, Weidong Jiang, Wei Wang, and Yan Gao. Investigation of zero sequence circulating current suppression for parallel three-phase grid-connected converters without communication. *IEEE Transactions on Industrial Electronics*, 65(10):7620–7629, 2018.

[60] L Wright and T J Esward. Fit for Purpose Models for Metrology: a Model Selection Methodology. *Journal of Physics: Conference Series*, 459:012039, September 2013.

[61] Zhihong Ye, D. Boroyevich, Jae-Young Choi, and F.C. Lee. Control of circulating current in two parallel three-phase boost rectifiers. *IEEE Transactions on Power Electronics*, 17(5):609–615, 2002.

[62] Akihiko Yoshikawa, Hiroyuki Matsunami, and Yasushi Nanishi. *Development and Applications of Wide Bandgap Semiconductors*, pages 1–24. Springer, 2007.

[63] Weibo Yuan, Yigang He, Bing Li, Jianbo Zhou, Zhiqiang Ma, and Chenchen Li. Improved cauer thermal network considering thermal coupling effects of multi-chip modules. *IET Power Electronics*, 13(16):3707–3716, 2020.

[64] Zicheng Zhang, Alian Chen, Xiangyang Xing, and Chenghui Zhang. A novel model predictive control algorithm to suppress the zero-sequence circulating currents for parallel three-phase voltage source inverters. In *2016 IEEE Applied Power Electronics Conference and Exposition (APEC)*, pages 3465–3470, 2016.